Atmospheric new particle formation in the eastern region of China: an ~~mechanistic~~ investigation on mechanism and influencing factors at multiple sites

Jiaqi Jin[1], Runlong Cai[1,2,3,4], Yiliang Liu[1,a], Gan Yang[1], Yueyang Li[1], Chuang Li[1], Lei Yao[1,2,3,4], Jingkun Jiang[5,6], Xiuhui Zhang[7], Lin Wang[1,2,3,4,8]

[1]Department of Environmental Science and Engineering, Jiangwan Campus, Shanghai Key Laboratory of Atmospheric Particle Pollution and Prevention (LAP[3]), Fudan University, Shanghai 200438, China

[2]Shanghai Institute of Pollution Control and Ecological Security, Shanghai 200092, China

[3]IRDR International Center of Excellence on Risk Interconnectivity and Governance on Weather/Climate Extremes Impact and Public Health, Fudan University, Shanghai, China

[4]National Observations and Research Station for Wetland Ecosystems of the Yangtze Estuary, Shanghai, China

[5]State Key Joint Laboratory of Environmental Simulation and Pollution Control, School of Environment, Tsinghua University, Beijing, China.

[6]State Environmental Protection Key Laboratory of Sources and Control of Air Pollution Complex, Beijing, China.

[7]Key Laboratory of Cluster Science, Ministry of Education of China, School of Chemistry and Chemical Engineering, Beijing Institute of Technology, Beijing, China.

[8]Collaborative Innovation Center of Climate Change, Nanjing, 210023, China

[a]now at Chongqing Institute of Green and Intelligent Technology, Chinese Academy of Sciences, Chongqing 400714, China.

Correspondence to: Lin Wang (lin_wang@fudan.edu.cn)

Abstract. As a major source of cloud condensation nuclei, atmospheric new particle formation (NPF) events exert significant influences on the global climate. Among ~~the various~~ nucleation mechanisms ~~that have been~~ identified in diverse environments, sulfuric acid-amine nucleation is unique for its high efficiency ~~to~~ in forming stable clusters and driving~~e~~ intense nucleation. Despite the fact that this nucleation mechanism ~~could~~ can explain observed NPF events at ~~a number of megacity sites in China~~individual sites, its applicability to a larger regional scale remains unclear. Here, we analyze~~d~~ the mechanism and influencing factors~~characteristics~~ of NPF ~~events~~ ~~and influencing factors~~ at several ~~three suburban~~ sites in the eastern region of China, ~~based on~~using measured and theoretically predicted particle formation rates and cluster concentrations. Results show that sulfuric acid and ~~-~~dimethylamine can explain the observed atmospheric nucleation and~~is a predominant nucleation mechanism at these sites, while~~ atmospheric conditions including precursor concentrations and temperature cause~~s~~ the differences in NPF characteristics among ~~different~~ sites. This indicates the significance of the sulfuric acid-amine nucleation ~~mechanism~~ over a large spatial scale in polluted and populated ~~the urban agglomerations in the eastern~~ region ~~of China~~s. We also find that oxygenated organic molecules are likely involved in the formation of 1.7-nm new particles at these sites by contributing the initial growth of stable sulfuric acid clusters.

1 Introduction

New particle formation (NPF), an important atmospheric process involving the conversion of gaseous precursors into stable clusters via nucleation and subsequent growth, occurs frequently in diverse environments (Kerminen et al., 2018). It is a large source of the number concentration of atmospheric particles and significantly influences the budget of global cloud condensation nuclei (Gordon et al., 2017). ~~Strong NPF events are frequently observed in polluted environments against the significant suppressing effect of background aerosols (Xiao et al., 2015; Hong et al., 2023).~~ Among a number of recently proposed nucleation mechanisms ~~that were proposed recently~~ (Kirkby et al., 2023), the ~~clustering~~ collision between sulfuric

acid (SA) and dimethylamine (DMA) is special for its high efficiency in forming clusters that are stable against evaporation, and has been found to be ~~a~~ the governing nucleation mechanism in polluted megacities~~ for its high efficiency in forming clusters that are stable against evaporation~~ (Yao et al., 2018; Cai et al., 2021). These findings corroborated prior studies conducted in urban Tecamac (Smith et al., 2010) and Atlanta (Hanson et al., 2011), where aminium salts were identified as a dominant constituent of sub-10 nm particles. Despite substantial suppression by background aerosols, strong NPF events were observed globally in polluted environments, though the underlying mechanisms often remain unclear (Nieminen et al., 2018). ~~Recently, a~~ A ~~relevant~~ recent model study (Zhao et al., 2024) ~~has~~ indicated that SA-~~DMA~~ amine ~~is still~~was the main nucleation mechanism in the polluted atmospheric boundary layers~~s~~ ~~of the polluted atmosphere on a~~across larger region~~al scales, such as ~1M km^2 the population dense area in the eastern region of China (Kulmala et al., 2021)~~. However, this regional-scale dominance requires evidence from field~~it remains to be explored through actual~~ ~~–~~measurements.

Atmospheric NPF is often a regional-scale phenomenon spanning hundreds of kilometers (Kerminen et al., 2018). Simultaneous measurements at two or more stations have demonstrated the spatial heterogeneity of regional NPF characteristics such as event~~the~~ frequency~~ of NPF events~~, ~~the~~ start time~~ and~~, duration, and~~ of NPF events, and~~ the formation and growth rates of new particles (Bousiotis et al., 2021; Zhou et al., 2021; Dinoi et al., 2023~~; Shang et al., 2023~~). This heterogeneity of NPF ~~is~~ may be associated with the spatially ~~heterogeneous~~ variable distributions of ~~diverse~~ emission sources, complex~~ urban~~ morphology and meteorology, and the ~~high~~ strong selectivity and sensitivity of NPF to atmospheric conditions. The main causes of variations in the macroscopic characteristics of NPF ~~remain~~ require ~~to be~~ further ~~verified~~verification, necessitating mechanistic investigations across~~. This urges a mechanistic exploration of NPF on a large~~ large ~~regional~~ regions~~scale, specifically, at multiple sites in the vast eastern part of China~~.

~~The influence of a~~A number of influencing factors need~~s~~ to be accounted for when resolving nucleation mechanisms in the real atmosphere. Besides the concentrations of gaseous precursors and the scavenging loss of clusters and particles characterized by the condensation sink (CS), temperature effects on ~~also influences nucleation by altering the stability of~~ cluster~~s~~ stability against evaporation (Olenius et al., 2017; Li et al., 2023). A ~~Global~~ global ~~nucleation~~ simulation study ~~using a three-dimensional model~~ suggest~~s~~ed that temperature was the second most important factor in nucleation, following the concentration of precursors (Zhao et al., 2024). Laboratory studies ~~have~~ provided experimental evidence for the ~~temperature~~ dependence of sulfuric acid-amine nucleation on temperature at atmospheric-relevant amine concentrations (Xiao et al., 2021). Previous ~~1~~one-year measurements in urban Beijing showed that temperature governed ~~the~~ seasonal ~~–~~variations of NPF frequency and particle formation rate (Deng et al., 2020). This also indicates that the intensity and characteristics of NPF likely vary on a large spatial scale, e.g., the characteristics of NPF in temperate (Cai et al., 2021) and tropics (Sebastian et al., 2021) regions can be different, even though the NPF events were governed by the same nucleation mechanisms.~~It is also reasonable to expect a temperature dependence of NPF on a broad spatial scale, which remains to be addressed by observations.~~

The initial growth of freshly nucleated particles is important for NPF, as these smallest particles are ~~most~~ highly susceptible to scavenging losses. Previous studies proposed that SA and its clusters ~~governs~~ significantly contributed to the initial growth in ~~Chinese megacities~~urban areas, although ~~the~~ contributions ~~from~~ of other condensable vapors, like oxygenated organic molecules (OOMs), could not be excluded (Yao et al., 2018; Deng et al., 2020). OOMs~~ were reported as~~ are identified as highly ~~the most~~ important precursors for the subsequent growth of particles. Observational evidence from remote forests ~~has demonstrated~~suggested that the volatility distribution of OOMs~~ can~~ reasonably accounted for particle growth from 3 to 50 nm (Mohr et al., 2019). Similarly, in urban environments, a substantial ~~proportion~~ fraction of particle growth ~~occurring~~ above 3 nm ~~has been~~was attributed to the condensation of OOMs (Qiao et al., 2021), indicating their ~~ubiquitous~~ key role in both anthropogenically influenced and natural settings. Moreover, insights from ~~controlled~~ chamber studies ~~also reinforced~~further supported the potential role of OOMs in growth of newly-formed particles. ~~In particular, s~~Some extremely low-volatility OOMs ~~have been shown~~can~~ to~~ promote directly to the ~~sub-3 nm~~ initial growth of sub-3 nm particles (Tröstl~~Troestl~~ et al., 2016; Stolzenburg et al., 2018). ~~According to the results from l~~Laboratory~~ies~~y results indicated that~~, the~~ ~~contribution of~~ OOMs contributions to the initial growth of new particles ~~is~~ are likely ~~to be~~ non-negligible in the real atmosphere, however, ~~there has been insufficient~~ ambient evidence for this process remains limited~~suggestion~~.

To deepen the understanding of NPF in polluted atmospheres, we collected data measured at three suburban~~ sites~~ sites and two urban sites in the eastern part of China, including SA and DMA concentrations ([SA] and [DMA]), OOMs

concentrations ([OOMs]), cluster compositions, and particle size distribution (PSD) down to ~1 nm. The ~~NPF~~ nucleation mechanisms ~~are~~ were analyzed after accounting for the effects of temperature and precursor concentrations on cluster concentrations and particle formation rates. Additionally, ~~We~~ we ~~also discuss~~ investigated the initial growth of new particles and explored the roles of OOMs in the formation of 1.7 nm particles.

2 Methods

2.1 Measurements

We conducted field campaigns at three suburban sites, namely Wangdu (WD), Dianshan Lake (DL) and Taihu Lake (TL). WD is located in Baoding, Hebei, with farmlands, forests and two major roads~~highways~~ nearby~~. (Wang et al., 2020; Hu et al., 2022; Ren et al., 2022).~~ DL is located in the southwest of Shanghai, surrounded by residential buildings, vegetation, a ~~main traffic artery~~highway and a few industrial enterprises~~ (Wu et al., 2023; Yang et al., 2023; Deng et al., 2025)~~. Two campaigns were conducted at DL, one in winter (DLW) and the other in spring (DLS). TL is located in Wuxi, Jiangsu, surrounded by vegetation and a small number of settlements. The detailed information of these campaigns is given in Table 1. Furthermore, this study also involves ambient data previously reported from urban sites, namely Shanghai (SH, Yao et al., 2018) and Beijing (BJ, Cai et al., 2021; Qiao et al., 2021). The location of these five sites is shown in Figure S1.

A chemical ionization long time-of-flight mass spectrometer (CI-LToF-MS, Aerodyne Research, Inc.) was deployed to measure gaseous SA, OOMs, and molecular clusters at ~~these three~~ three suburban sites (Lu et al., 2020)~~. The mass spectrometer, used~~ using nitrate and its clusters to ionize neutral molecules and clusters. A calibration coefficient derived from SA and a mass-to-charge-dependent transmission efficiency of the instrument were used to obtain [OOMs], assuming that they share the same kinetically controlled collision rate with reagent ions as that of SA. The transmission efficiency was calibrated using a system coupling a high-resolution differential mobility analyzer (HR-DMA) with the mass spectrometer (Heinritzi et al., 2016). The calibrations of [SA] and transmission efficiency were performed before each campaign.

A Vocus proton-transfer-reaction time-of-flight mass spectrometer (Vocus PTR-ToF-MS, Aerodyne Research Inc.) equipped with a focusing ion-molecular reactor (FIMR) was used at WD and DL, with modified instrument settings to measure DMA (Wang et al., 2020). A chemical ionization high-resolution time-of-flight mass spectrometer (CI-HToF-MS, Aerodyne Research Inc.) was used at TL, with protonated ethanol or its hydrated clusters as reagent ions~~ (Yao et al., 2016)~~, to measure DMA (Yao et al., 2016). Since mass spectrometer cannot distinguish among isomers, C_2-amine was taken as DMA. NH_3 concentration ([NH_3]) was measured using the ion chromatography (IC) method of Chinese Standard (HJ 1076-2019) at WD and DL. There was no measurement for [NH_3] at TL. The detailed measurement methods for these chemical species are given in the Supplement.

Particle size distribution (PSD) ranging from 1 to 3 nm was measured by an Airmodus A10 particle size magnifier (PSM). The PSD of 3-736 nm particles was measured by two scanning mobility particle sizers (SMPS TSI Inc, USA), namely a nano-SMPS and a long-SMPS (Yao et al., 2018). Temperature was monitored by an automatic weather station (Vaisala AWS310).

~~Furthermore, this study also involves ambient data previously reported at urban sites, namely Shanghai (SH, Yao et al., 2018) and Beijing (BJ, Cai et al., 2021; Qiao et al., 2021).~~

Table 1: The location, period and the usage of instrument at different sites.

Site	Location	Period	Instrument			
			SA & OOMs	DMA	NH_3	PSD
WD	38°39’ N, 115°11’ E	Dec. 2018-Jan. 2019	CI-LToF-MS	Vocus PTR-ToF-MS	CI	nano-SMPS+ long-SMPS+
DL	31°05’ N, 120°59’ E	Dec. 2022-Jan. 2023 & Apr. 2023-Jun. 2023				

TL	31°25’ N, 120°13’ E	Jul. 2023-Sep. 2023	HToF-CIMS	Not available	PSM

2.2 Models

A cluster dynamics-multicomponent sectional model was applied to simulate SA-DMA nucleation process (Li et al., 2023). The model is composed of one cluster dynamics module and one sectional module. The detailed description of these two modules is given in the Supplement. SA tetramers were treated as nucleated particles for simulating particle formation rate at 1.4 nm diameter, $J_{1.4}$ (Larriba et al., 2011~~; Cai et al., 2021~~), and entered the sectional module as the smallest particles. Particle formation rate at 1.7 nm diameter, $J_{1.7}$, was simulated by incorporating the initial growth on the basis of $J_{1.4}$. However, in certain cases, this process could not be directly implemented in the model, because of data overflow~~.~~ (Figure ~~S1~~S2). Therefore, a survival probability approach was adopted as an alternative ~~for the calculation~~ (Cai et al., 2022a):

$$\frac{J_{\mathrm{p}_1}(t)}{J_{\mathrm{p}_2}(t)} = \exp\int_{d_{\mathrm{p}2}}^{d_{\mathrm{p}1}} -\frac{\mathrm{CoagS}(d_{\mathrm{p}})}{\mathrm{GR}(d_{\mathrm{p}})}\,\mathrm{d}d_{\mathrm{p}} \tag{1}$$

where d_{p1} is 1.7 nm, and d_{p2} is 1.4 nm, the corresponding particle size in calculating particle formation rates. The ratio $J_{1.4}/J_{1.7}$ is defined as the survival probability from 1.4 nm to 1.7 nm. GR is herein the simulated size-dependent growth rate, which is contributed by condensable vapors through the change of particle mass over time:

$$\frac{\mathrm{d}m_{\mathrm{p}}}{\mathrm{d}t} = \sum_i m_i\left(\alpha\beta_i N_i - \beta_i N_{i,\mathrm{sat}}\exp\left(\frac{4v_i\sigma}{d_{\mathrm{p}}k_{\mathrm{B}}T}\right)f_i\right) \tag{2}$$

where m_{p} is the mass of particle; i represents each condensable species; m_i is the mass of molecules or clusters; α is the accommodation coefficient, β_i is the collision constant between species i and the particle; $N_{i,\mathrm{sat}}$ is the saturation concentration; v_i is the molecular volume, σ is the surface tension of the particle; k_{B} is the Boltzmann constant; and f_i is the molar fraction in the particle. In calculations, ~~$(SA)_{1-4}(DMA)_{0-4}$ was treated as non-evaporative, meaning that they do not return to the gas phase after condensing on the particle.~~the fragmentation of SA-DMA clusters from particles was taken to be negligible, i.e., clusters did not return to the gas phase after coagulating onto a particle.

2.3 Uncertainty analysis

The uncertainty of SA monomer concentration ($[SA_1]$) was estimated to be +100%/-50% (Cai et al., 2021). The uncertainty of [DMA] was +150%/-60% taking into account systematic and calibration uncertainties among campaigns (Freshour et al., 2014). The uncertainty of [OOMs] was expected to be greater than that of $[SA_1]$, because it was quantified by the calibration factor of SA. Li et al. (2023) reported that [OOMs] with a scaling factor of 1.35-4 could explain the measured new particle growth. Hence, the uncertainty of OOMs was estimated to be +200%/-66%. In terms of the volatility estimation of OOMs, the logarithm of saturation mass concentration ($\log C^*$) had an uncertainty of ±1 (Stolzenburg et al., 2018). The ~~uncertainty~~ uncertainties of CS and measured ~~-~~particle formation rate were ±10~~-~~% and +100%/-50%, respectively (Cai et al., 2021). All uncertainties of these parameters are listed in Table S1.

The uncertainties of simulated values, like the SA dimer concentration ($[SA_2]$) and the particle formation rate were obtained by inputting the ~~extreme values of the~~ uncertainty ranges of measured data into the model. For example, the measured value of $[SA_1]$, [DMA] and CS were scaled by factors of 2, 2.5, and 1.1 (according to their uncertainty) were input to calculate the upper boundary of the uncertainty range of simulated $[SA_2]$ ($[SA_2]_{\mathrm{sim}}$) and simulated $J_{1.4}$ ($J_{1.4,\mathrm{sim}}$) and the lower boundary of simulated value was calculated in a similar way to the upper boundary, except that scale factors of 2, 2.5 and 1.1 were replaced by 0.5, 0.4 and 0.9, respectively.

2.4 Scaling processing

To quantitatively characterize the effects~~In order to better visualize the effects~~ of $[SA_1]$ and temperature on $[SA_2]$ ~~SA dimer concentration~~ and particle formation~~nucleation~~ rate, we normalized~~accounted~~ the effects of CS and [DMA] by scaling the measured values to consistent conditions~~a same level~~ based on simulation. Here, the scaling of measured $[SA_2]$ ($[SA_2]_{\mathrm{meas}}$)

is ~~given~~ defined as ~~an example~~follows:

$$[SA_2]_{scaled} = [SA_2]_{meas} \cdot C(CS_{median}, [DMA]_{median}) \quad (3)$$

where $[SA_2]_{scaled}$ refers to the scaled $[SA_2]_{meas}$; $C(CS_{median}, [DMA]_{median})$ is the scaling coefficient for $[SA_2]_{meas}$, and was calculated by:

$$C(CS_{median}, [DMA]_{median}) = \frac{[SA_2]_{sim,median}}{[SA_2]_{sim}} \quad (4)$$

where $[SA_2]_{sim}$ ~~is~~denotes the simulated SA_2 concentration ~~, which was~~ calculated by inputting measured $[SA_1]$, [DMA], CS and temperature into the cluster dynamics-multicomponent sectional model; $[SA_2]_{sim,median}$ ~~is~~was calculated using measured $[SA_1]$ and temperature, combined with~~by inputting measured $[SA_1]$, measured temperature,~~ the median [DMA] (2.3 pptv) and the median CS (0.017 s^{-1}) ~~of~~in all NPF events. $[SA_2]_{sim,median}$ ~~can be~~is regarded as the theoretical $[SA_2]_{meas}$ when measured [DMA] and CS attain~~reach~~ their event median ~~values~~s. [DMA] was unavailable~~not measured simultaneously with [SA]~~ at SH. Considering high [DMA] (0.7-54.3 pptv) in other campaigns in urban Shanghai (Yao et al., 2016; Chang et al., 2021), a fixed [DMA] ~~at SH~~ (5 pptv) was ~~uniformly~~ set ~~at 5 pptv in~~for scaling, ~~at which $[SA_2]$~~ almost reaching~~ed~~ the nucleation limit under the atmospheric $[SA_1]$ (Almeida et al., 2013). The analogous scaling methodology for~~of the~~ particle formation rates is ~~given in~~ detailed in the Supplement.

3 Results and discussion

3.1 SA-DMA nucleation for all the campaigns

SA and DMA can explain the atmospheric nucleation observed at all sites. This finding is supported by the correlation between $[SA_1]$ and particle formation rates, the composition of detected clusters, the alignment of simulated and measured nucleation intensity ($[SA_2]$ and particle formation rates), and the dependences of NPF on temperature and [DMA]. The first two points are addressed in this section, while the remaining evidence will be discussed in Sect. 3.2 and Sect. 3.3.

Figure 1 shows the measured particle formation rates at 1.7 nm diameter ($J_{1.7,meas}$) as a function of $[SA_1]$ and compares them with~~-~~ those in other studies~~measured results of other campaigns~~. All measured particle formation rates are much higher than SA-NH_3 at corresponding temperatures of Cosmics Leaving Outdoor Droplets (CLOUD) experiments, which suggests the existence of precursors with higher basicity, like amines (Kirkby et al., 2011; Almeida et al., 2013). Our data (~~,~~ except ~~for that at~~ TL~~,~~) is in accordance with SA-DMA-NH_3(-OOMs) nucleation at 293 K of ~~Cosmics Leaving Outdoor Droplets (~~CLOUD, even though the median temperature in our campaigns was 287 K~~) experiments~~. Data ~~at~~ from TL follows the simulated line~~s~~ for SA-DMA nucleation at 303 K. Furthermore, our observed results align closely with~~are also close to~~ those at SH and BJ, where SA and DMA have been suggested to be key nucleating precursors~~proved to play key roles in nucleation~~ (Yao et al., 2018; Cai et al., 2021), indicating a potentially consistent~~meaning that~~ nucleation mechanism~~s~~ across these locations~~among them are very likely to be consistent~~. Compared with CLOUD experimental conditions (Table 2), ou~~Ou~~r campaigns exhibited ~~had~~ higher CS and lower [DMA]~~than the~~, b~~experimental conditions of CLOUD (Table 2), b~~oth of which ~~are~~ were unfavorable for ~~$J_{1.7}$~~NPF. This explains ~~provides an explanation for~~ the generally lower particle formation rates ~~$J_{1.7,meas}$~~ observed in our measurements relative to those from CLOUD~~compared to those from CLOUD~~ under varying temperature conditions. ~~Particle formation rates under SA-DMA nucleation remain almost unchanged after adding certain $[NH_3]$ and [OOMs] in CLOUD (Kürten et al., 2018; Xiao et al., 2021), and our observations show a close level of $[NH_3]$ and relatively low [OOMs] compared with CLOUD experiments (Table 2). It is difficult to determine whether NH_3 and OOMs participate in nucleation based on particle formation rate solely.~~ Therefore, the observed nucleation is likely driven by SA and enhanced by strong stabilizing precursors such as DMA. Other nucleation mechanisms are unlikely to dominate under these conditions.~~the dominate NPF mechanism in our campaigns was identified as SA-DMA.~~

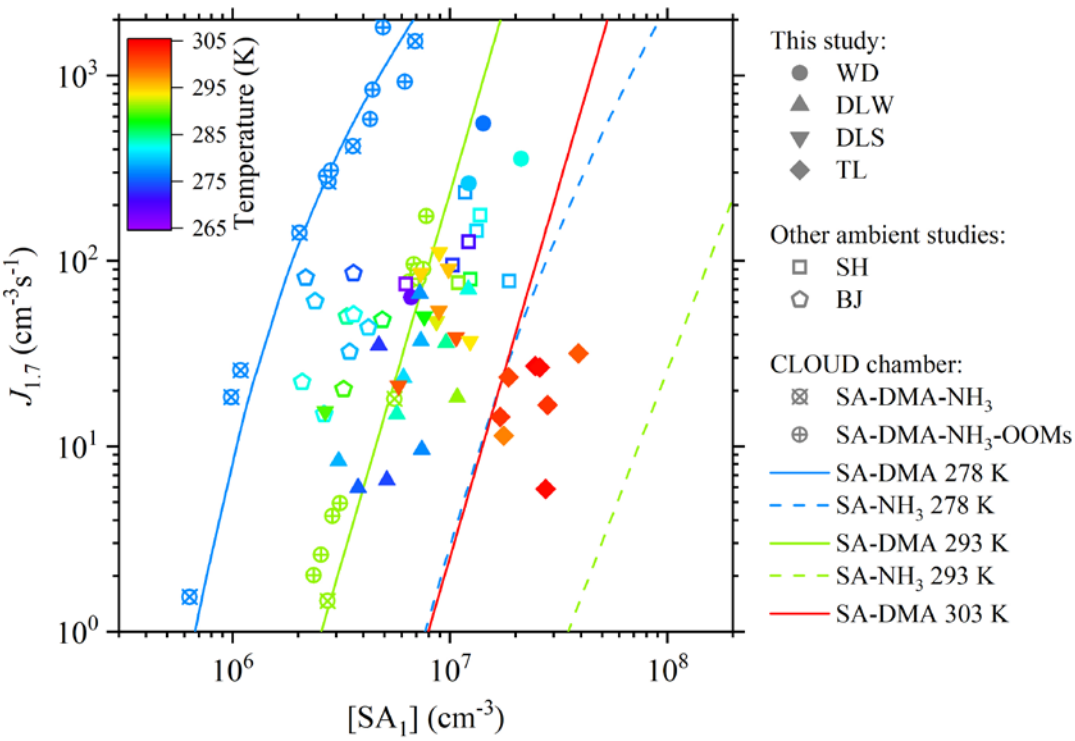

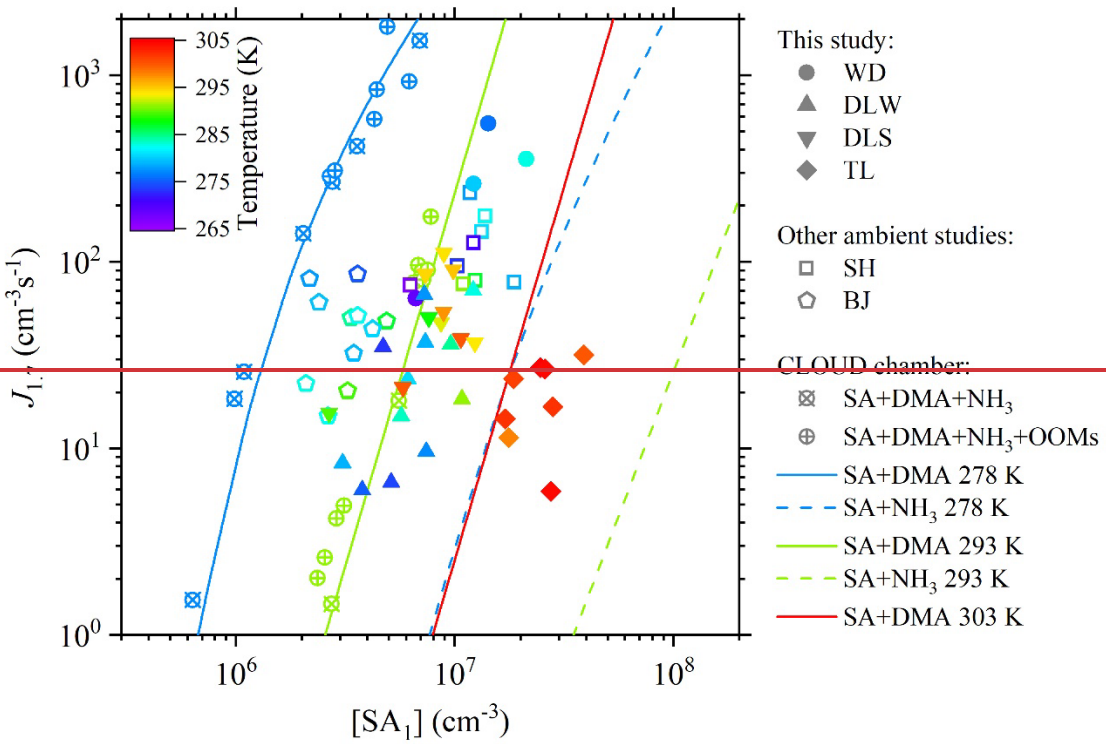

Figure 1: $J_{1.7,meas}$ as a function of [SA$_1$] with the comparison of ambient data and CLOUD. Rainbow filled symbols represent measured data in this study, indicating one NPF events with the time resolution of 30 min, which were selected when $J_{1.7,meas}$ reaches maximum. Rainbow open symbols represent data from published studies (Yao et al., 2018; Cai et al., 2021). Symbols with crosses indicate CLOUD data in the temperature of 278 K and 293 K, respectively. Lines represent the fitting result of CLOUD (Xiao et al., 2021), except for the SA-DMA fitting at 303 K that is derived from the CLOUD fitting line of SA+DMA 293 K by the cluster dynamics-multicomponent sectional model.

Table 2: Comparison of NPF characteristics in different campaigns.

~~Dada~~ Data source		Temperature (K)	CS (s^{-1})	[DMA] (pptv)	[OOMs] (cm^{-3})	[NH_3] (ppbv)
This study	median	290	0.017	2.3	1.8×10^{8}	2.1
	range	268-307	0.008-0.060	0.6-18.3	2.0×10^{7}-9.7×10^{8}	0.4-7
CLOUD (Xiao et al., 2021)		278, 293	0.002-0.008	4	up to 8.8×10^{9}	1-2.5
Shanghai (Yao et al., 2018)		267-291	0.017-0.039	not available	2.3×10^{7}-2.1×10^{8}	not available
Beijing (Cai et al., 2021; Qiao et al., 2021)		275-289	0.005-0.021	0.7-3.5	1.2×10^{7}-6.4×10^{7}	0.3-2.3

The composition of the measured cluster~~ composition~~ provides ~~observational~~ further evidence for the involvement of DMA in the formation of SA clusters~~, while other base molecules were not detected~~ (Figure 2). A number of neutral clusters, including SA and SA-DMA clusters, ~~along with S-O based ions,~~ were observed at WD, DL and TL. These clusters are described as SA monomer (SA_1), dimer (SA_2), trimers (SA_3DMA_{0-2}) and tetramers (SA_4DMA_{1-2}), contributing to NPF. The absence of DMA in pure SA ~~monomer and dimer~~ clusters can be attributed to in-situ fragmentation with~~are caused by their loss~~ in the mass spectrometer (Alfaouri et al., 2022~~Cai et al., 2022b~~), suggesting more DMA molecules were expected to be existed in clusters. Similar patterns of SA-DMA clusters were also measured by CI-TOF-MS in other urban sites~~at SH~~ (Yao et al., 2018~~)~~ ~~and BJ (~~; Yin et al., 2021). Besides, the normalized signal of SA trimer and tetramer show good correlations (r^2 = 0.44-0.76) with the number concentration of sub-3 nm particles (Figure S3). Such correlations between clusters and newly formed particles were reported in other atmospheric observations (Bianchi et al., 2016; Yan et al., 2021), indicating that these clusters typically signified the molecular clustering processes in NPF events. Other molecules that may ~~clusters related to nucleation, like SA-OOMs and SA-NH_3, were not observed, but the possibility that NH_3 and OOMs~~ participate in nucleation~~ cannot be ruled out,~~ , such as OOMs and NH_3, were not detected in clusters, as they are generally in the form of~~as they are generally present in the detection of~~ ion clusters~~,~~ rather than neutral clusters (Bianchi et al., 2016; Yin et al., 2021; Cai et al., 2024).~~ The accordant comparison of simulated and measured [SA_2], and the temperature dependence of nucleation also give further support for that SA-DMA nucleation, which is described specifically in the Sect. 3.2.~~

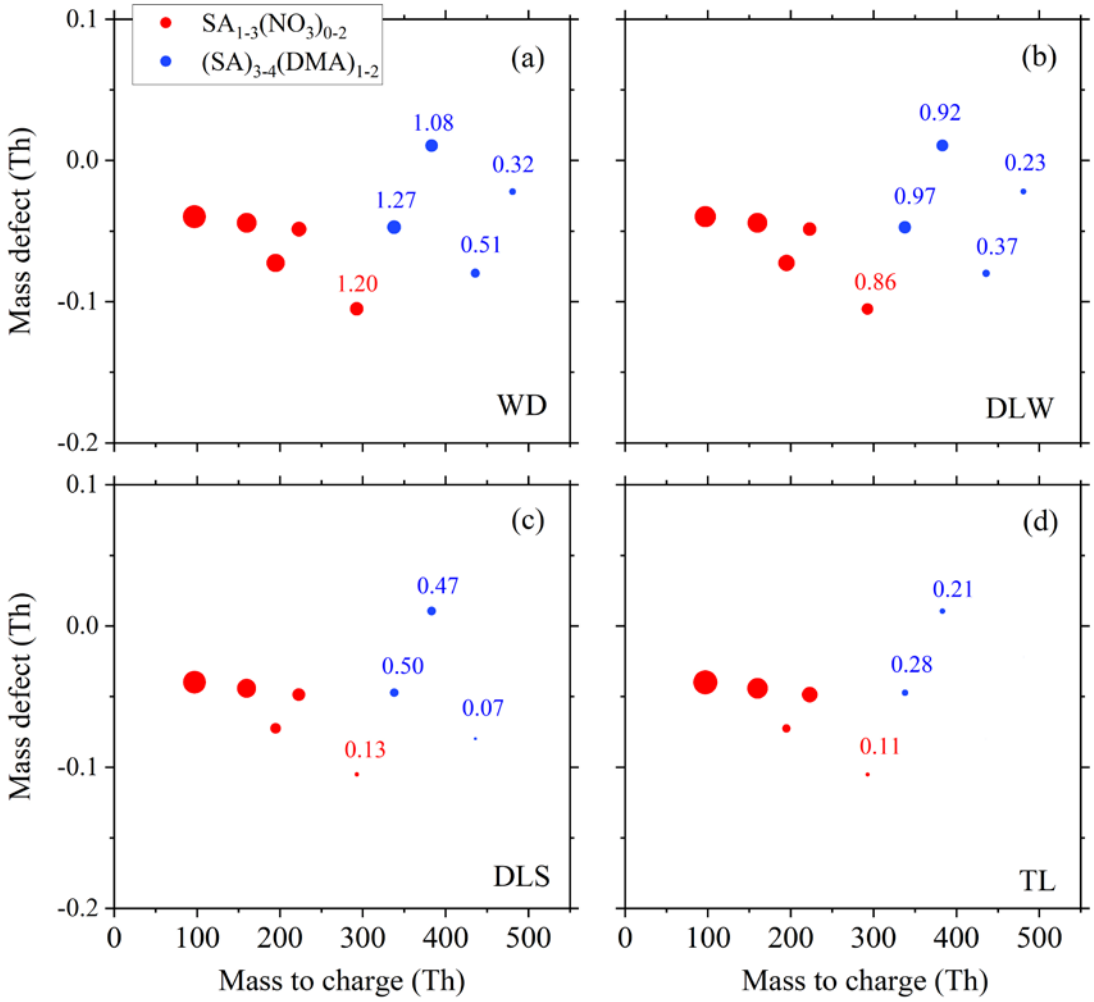
SA1-3(NO3)0-2
(SA)3-4(DMA)1-2
(a)
(b)
(c)
(d)
WD
DLW
DLS
TL
1.08
0.32
1.27
0.51
1.20
0.92
0.23
0.97
0.37
0.86
0.47
0.50
0.07
0.13
0.21
0.28
0.11
Mass defect (Th)
Mass to charge (Th)
0.1
0.0
-0.1
-0.2
0
100
200
300
400
500

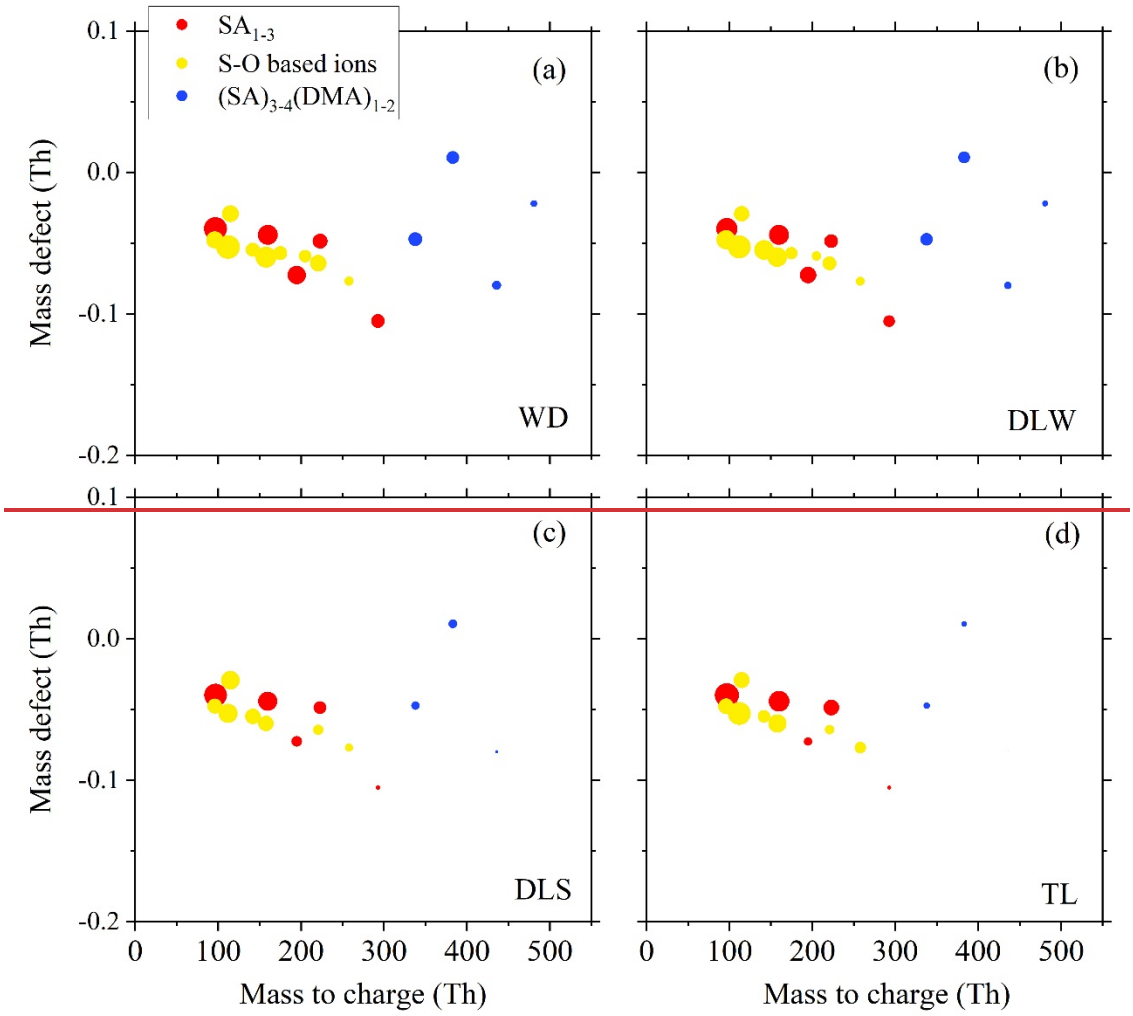

Figure 2: The mass defect of SA molecules and~~,~~ its clusters~~, and S-O based ions~~ during four NPF events on (a) January 20th, 2019 ~~in~~ at WD (temperature = 275 K; [SA_1] = 1.4×10^7 cm^{-3}; CS =0.055 s^{-1}; [DMA] = 3.4 pptv); (b) January 27th, 2023 ~~in~~ at DLW (temperature = 277 K; [SA_1] = 7.3×10^6 cm^{-3}; CS =0.012 s^{-1}; [DMA] = 1.5 pptv); (c) May 2nd, 2023 ~~in~~ at DLS (temperature = 295 K; [SA_1] = 9.5×10^6 cm^{-3}; CS =0.014 s^{-1}; [DMA] = 2.9 pptv); (d) August 7th, 2023 ~~in~~ at TL (temperature = 304 K; [SA_1] = 2.6×10^7 cm^{-3}; CS =0.023 s^{-1}; [DMA] = 1.8 pptv). Other species detected by CI-LToF-MS were not shown, because they are not directly related to atmospheric nucleation. The area of symbol ~~size~~ is proportional to the logarithm of ~~the~~ normalized signal ~~intensity~~. (multiplied by a factor of 1×10^6 before taking the logarithm). The logarithm of values is annotated for larger clusters.

3.2 The influencing factors of NPF

We ~~further~~ analyzed the factors determining the occurrence of NPF events in different campaigns by contrasting NPF and non-NPF events (Figure 3). [SA_1] during NPF periods was 0.5-2 times higher than that during non-NPF periods at~~is key to determining the occurrence of NPF at~~ DL and TL, suggesting [SA_1] was key to determining the occurrence of NPF at these sites~~ with the median values of [SA_1] being 1-2 times higher in NPF periods compared to those in non-NPF periods~~ (Figure 3a). This pattern resembles that observed in Barcelona (Brean et al., 2020) but differs from that observed in Beijing (Deng et al., 2020; Yan et al., 2021), where low CS was related to the occurrence of NPF without evident variations in [SA_1]. ~~Similarly,~~ CS during NPF periods ~~is~~ was generally lower than that during non-NPF ~~days~~ periods in all campaigns, except DLS, further confirming that high preexisting aerosols~~ are able to~~ suppressed the occurrence of NPF (Figure 3b). However, NPF events were not significantly dependent on the~~It contrasts with patterns in Po Valley, where~~ CS in Po Valley,~~ remained at similar levels regardless of whether NPF occurs~~ indicating other influencing factors govern the occurrence of NPF in less polluted atmospheres (Cai et al., 2024). Therefore, both the strength of precursor sources and pre-existing sink were important to the occurrence of NPF at our sites.

Besides SA, other ~~Other~~ potential precursors related to NPF in polluted regions ~~nucleation,~~ including DMA, NH_3 and OOMs ~~and NH_3 seem to have no notable influence on the occurrence of NPF in all campaigns,~~ (Figure S4). These species are known to enhance SA-driven nucleation (Kirkby et al., 2011; Almeida et al., 2013; Riccobono et al., 2014) and promote particle growth (Tröstl et al., 2016). Increasing [DMA] considerably enhances SA_2 formation under fixed temperature ranges (Figure S5), and this effect diminishes as [DMA] approaches nucleation saturation (Almeida et al., 2013). This phenomenon supports the contribution of DMA to atmospheric nucleation and is consistent with the results from a flow reactor (Jen et al., 2014). In CLOUD studies, the contributions of OOMs and NH_3 to cluster formation were almost negligible in the presence of DMA (Kürten et al., 2018; Xiao et al., 2021). Given that our field measurements exhibited similar [NH_3] and relatively low [OOMs] compared to those in CLOUD experiments (Table 2), it follows that their effects are also minor under our ambient conditions. Despite the potential participation of other precursors, the observation-simulation agreement suggests DMA is a major base that stabilizes SA clusters (Figure S5). However, [DMA] and [NH_3] were not markedly elevated during NPF periods (Figure S4). The likely reason is that the suppression of NPF by high CS masked the enhancing effect of DMA and NH_3, as they were positively correlated with CS (r^2=0.31 and 0.39, respectively, Figure S6). ~~since their concentrations during NPF periods were not obviously higher than those during non-NPF periods (Figure S2).~~

Although the occurrence of NPF is not strongly dependent on ambient temperature in individual campaigns (Figure 3c), the intercomparison across campaigns indicates a general negative correlation between NPF frequency and temperature, reflecting seasonal characteristics (Figure 3d). This trend is consistent with long-term measurements in Chacaltaya (Rose et al., 2015), Beijing (Deng et al., 2020) and Gwangju (Lee et al., 2024), where NPF was most frequent in winter and least frequent in summer. The intercomparison of campaigns further shows that temperature played a key role in determining the intensity of NPF indicated by [SA_2] and $J_{1.7,meas}$ (Figure 3e-f). Temperature even exerted more dominant influence than [SA1] and CS. For example. ~~Similarly, temperature does not appear to be a decisive factor determining the occurrence of NPF (Figure 3c), but it exerts a considerable influence on the intensity of NPF among campaigns, as elaborated in the next paragraph.~~

~~The comparison among different campaigns indicates that [SA_1] and temperature played key roles in determining the intensity of NPF indicated by $J_{1.7,meas}$ (Figure 3d). Although~~despite the highest [SA_1] at TL ~~is the highest at all sites~~, ~~high~~ its elevated temperatures (298-306 K) ~~at TL~~ resulted in lower median values of [SA_2]~~meas~~ and $J_{1.7,meas}$ than those in all campaigns~~at other sites~~. Conversely~~In contrast~~, WD ~~has~~ had the lowest temperature (281-268 K) and relatively high [SA_1] (7×10^6-1.8×10^7 cm^{-3}) ~~in all campaigns.~~, the intensity of NPF at WD was the highest, ~~Even~~ even under strong coagulation scavenging ~~effect~~ (median CS = ~0.05 s^{-1})~~, $J_{1.7,meas}$ at WD are the highest (~310 $cm^{-3}s^{-1}$)~~. A more detailed discussion regarding the influence of temperature on NPF is provided in Sect. 3.3.~~The effect of temperature on NPF was also considerable in the analysis of other observations in Beijing in different seasons (Deng et al., 2020).~~

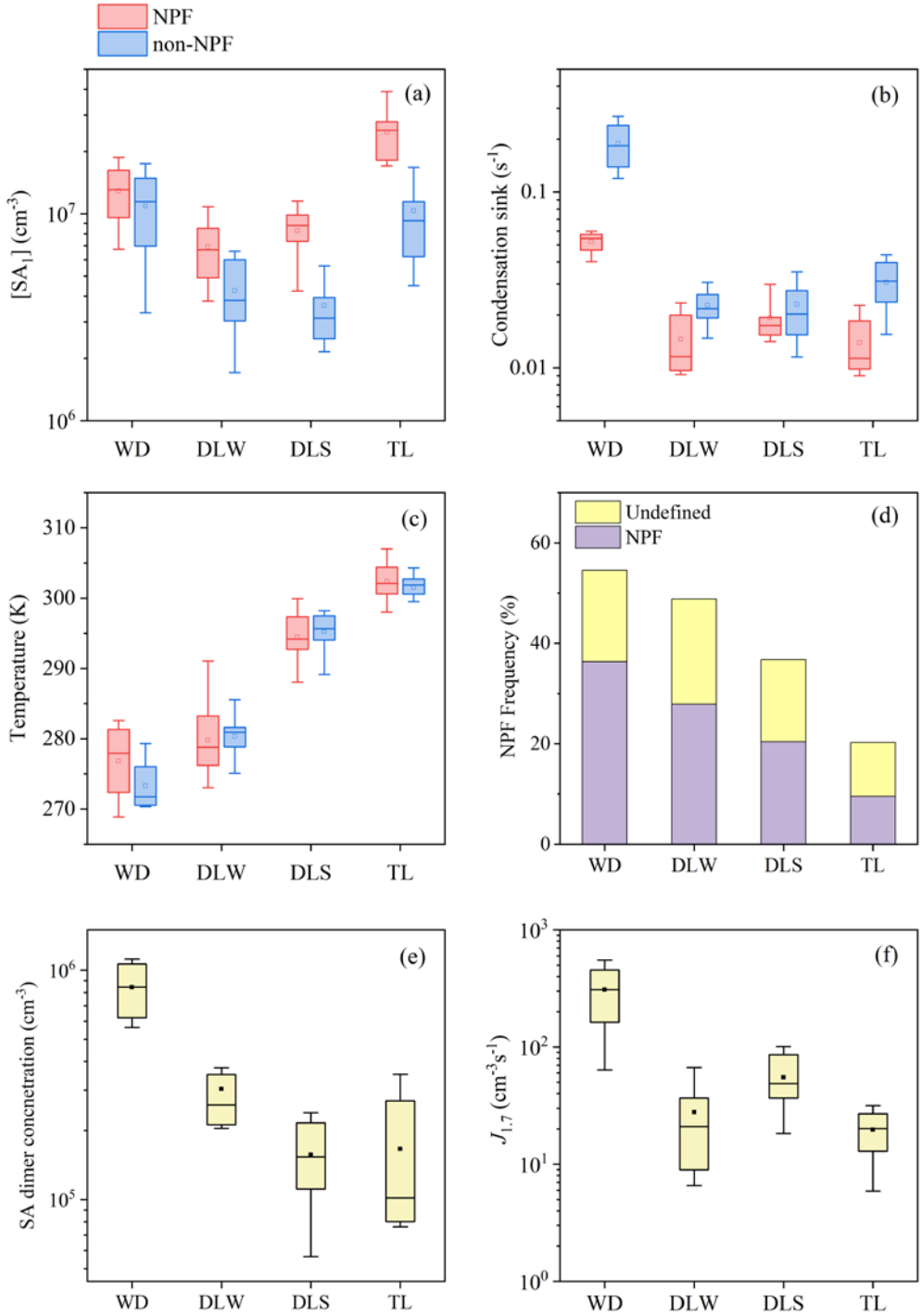
NPF
non-NPF
(a)
[SA1] (cm-3)
10^7
10^6
WD
DLW
DLS
TL
(b)
Condensation sink (s-1)
0.1
0.01
(c)
Temperature (K)
310
300
290
280
270
(d)
Undefined
NPF
NPF Frequency (%)
60
40
20
0
(e)
SA dimer concnetration (cm-3)
10^6
10^5
(f)
J1.7 (cm-3s-1)
10^3
10^2
10^1
10^0

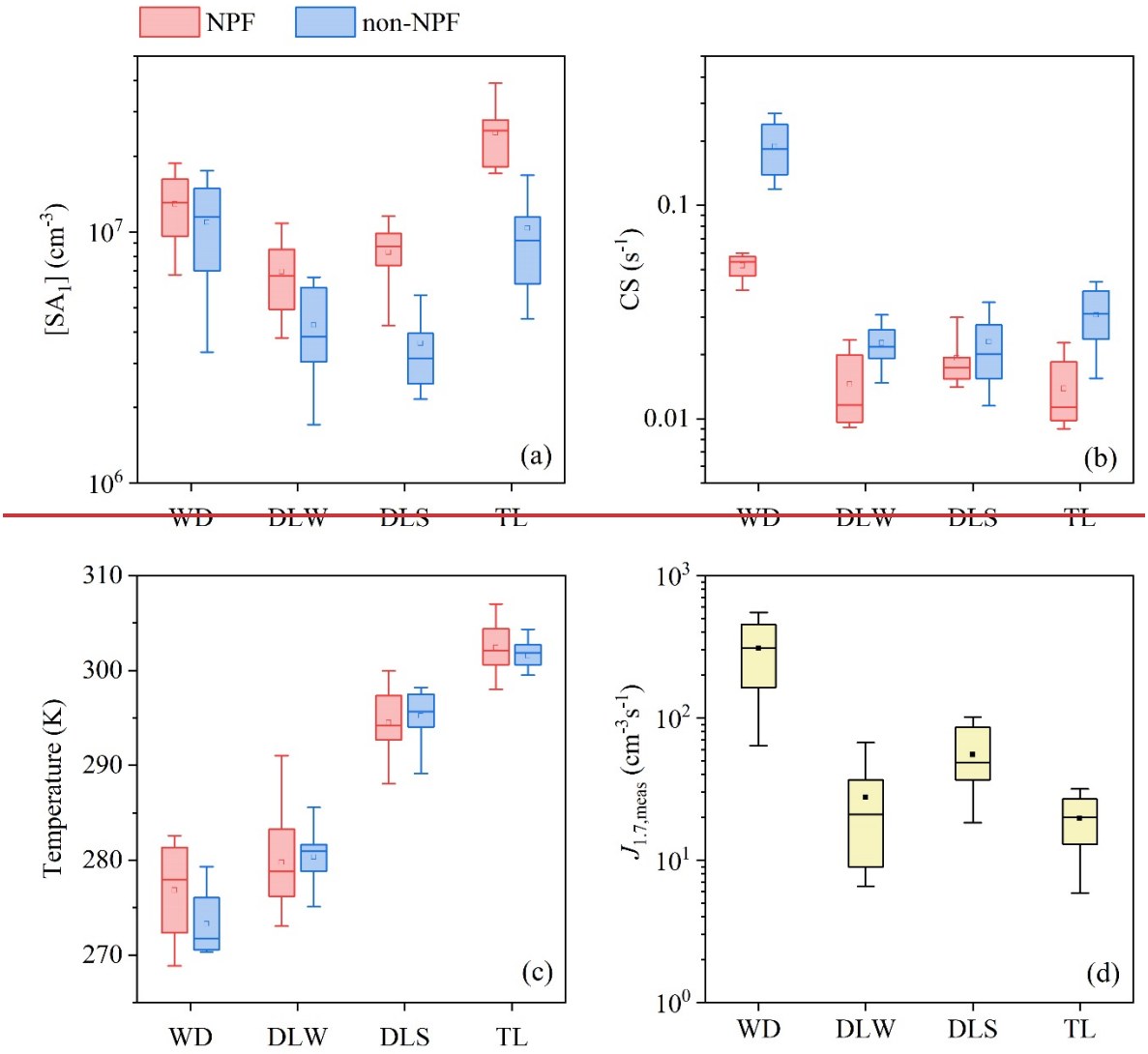

Figure 3: Parameters related to NPF. (a) [SA_1], (b) CS, (c) temperature during NPF periods and non-NPF periods, ~~and~~ (d) NPF frequency in each campaign, and (e) [SA_2] and (f) $J_{1.7,meas}$ during NPF periods. The NPF period is defined as the period with the maximum value of $J_{1.7}$ in each NPF event, and the non-NPF period is defined as the median range of all NPF periods (9:00-11:00) in non-NPF days. In order to eliminate the influence of precipitation, only sunny and cloudy days are selected for non-NPF. The transverse lines and square markers inside the boxes indicate mean values and median values, respectively. The bottom and top edges of the box indicate the 25th and 75th percentiles, respectively. The bottom and top edges of the whisker lines outside of the boxes indicate the 10th and 90th percentiles, respectively.

3.~~2~~ 3 The ~~Temperature~~ dependence of nucleation on temperature

~~To focus on the influence of [SA_1] and temperature on nucleation, and minimize the influence of other influencing factors, namely [DMA] and CS, on nucleation, we scaled the measured data to the median [DMA] and CS (see Methods).~~ Figure 4 shows that ~~the comparison between [SA_2]$_{sim}$ and~~ [SA_2]$_{meas}$~~,~~ is in accordance with [SA_2]$_{sim}$ when considering the uncertainties, indicating SA and DMA could explain the formation of SA_2.~~in which [SA_2]$_{meas}$ is in an agreement with the corresponding [SA_2]$_{sim}$, considering the uncertainty range in its measurement.~~ To be specific, ~~the~~ [SA_2]$_{meas}$ is slightly lower than [SA_2]$_{sim}$ overall.~~the simulated value,~~ Similar discrepancies between measured and simulated cluster concentrations have also been reported in CLOUD experiments (Kürten et al., 2014). This systematic underestimation is likely attributable to measurement errors, because not all SA_2 is fully detected, as some may dissociate within the mass spectrometer (Alfaouri et al., 2022).~~and this systematic discrepancy is likely due to measurement errors. It is possible that not all SA_2 is fully detected, as some of them~~

~~may have dissociated within the mass spectrometer (Zapadinsky et al., 2019).~~ The observation-simulation comparison of $J_{1.4}$ is shown in Figure S7, where simulation results fall within acceptable ranges upon uncertainty analysis. The consistency between measured and simulated parameters ([SA_2] and $J_{1.4}$) supports the significance of SA-DMA collision in NPF.

~~The comparison of measured and simulated $J_{1.4}$ is shown in Figure S3, and the simulation results are acceptable through uncertainty analysis. In addition to supporting our argument that SA-DMA clustering can explain the formation of stable SA dimers, this agreement between $[SA_2]_{sim}$ and $[SA_2]_{meas}$, also provides supports for the feasibility to use simulation for of data scaling.~~

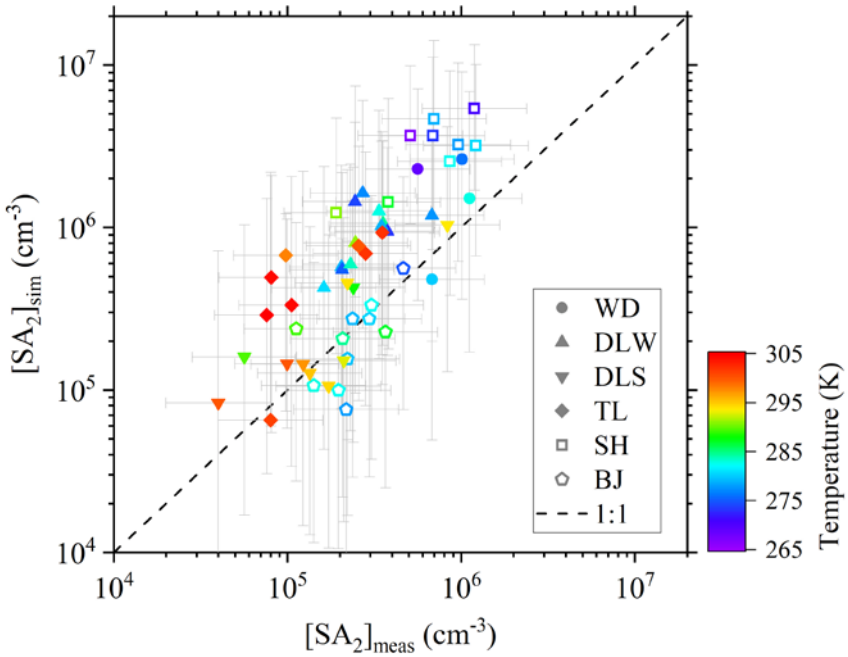

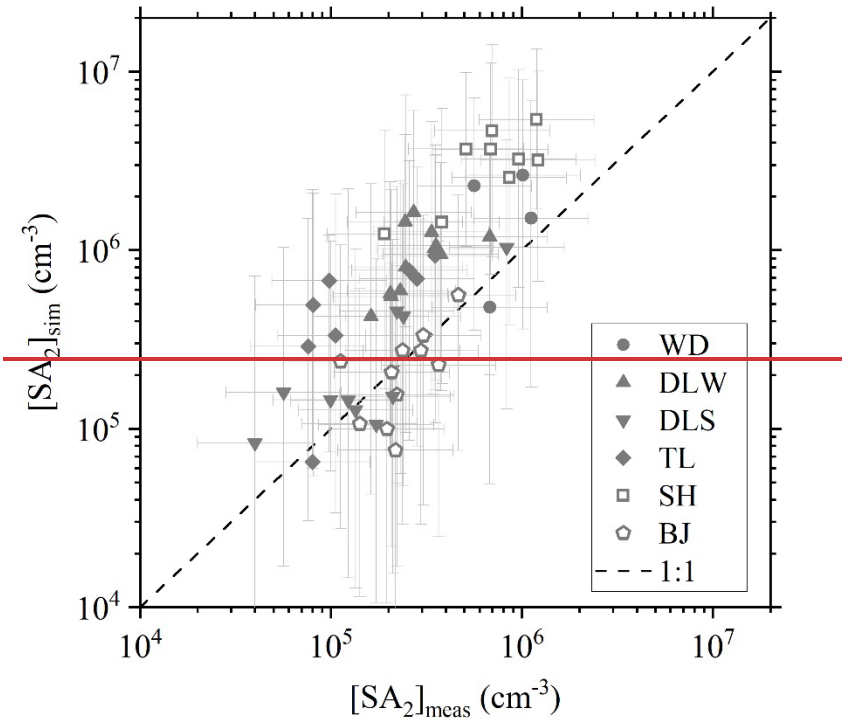

Figure 4: The comparison between $[SA_2]_{meas}$ and $[SA_2]_{sim}$. Horizontal and vertical error bars connected with each symbol indicate the uncertainties of x-axis and y-axis, respectively.

The consistency between measured and simulated parameters also validates the applicability of the model for data scaling. After accounting for the influences of CS and [DMA], ~~we find that~~ $[SA_2]_{scaled}$ ~~show~~ exhibits a significant decreasing trend with ~~an increar~~rising temperature, ~~which is in a decent consistency~~showing agreement with ~~the~~ simulated results (Figure 5). ~~For every 20 K increase in temperature, the $[SA_2]_{scaled}$ descends by approximately one order of magnitude.~~ This trend underscores the ~~dominant influence~~effect of temperature in governing the stability and abundance of clusters in nucleation pathways. ~~The temperature dependence of the ratio of $[SA_2]$ to $[SA_1]$ is also corroborated by previous studies focusing on SA-DMA nucleation. (Almeida et al., 2013; Yao et al., 2018). On~~At the molecular level, it is proposed that SA and DMA form ~~DMA acts as a kind of stable nucleating agent. Most of SA firstly converts into~~ SA_1DMA_1 clusters, which subsequently contributes to SA_2 formation, during nucleation~~and then forms SA dimer subsequently (Cai et al., 2022b). SA_1DMA_1 has relatively low thermal stability~~ (Olenius et al., 2017; Myllys et al., 2019). While SA_2 with one or two DMA molecules has been demonstrated to already be stable against evaporation (Jen et al., 2014), the formation of SA_1DMA_1 is a temperature-sensitive process that acts as the major rate-limiting step in clustering (Cai et al., 2022b). Kürten et al. (2016) and Brean et al. (2020) observed relatively low ratios of $[SA_2]$ to $[SA_1]$ (~0.01) at an urban site and a rural site, respectively, and speculated that they were related to higher temperatures (298-308 K).~~, which explains the temperature effect on $[SA_2]$ mechanistically.~~

An intercomparison of the panels in Figure 2 shows that the abundance and variety of larger SA-DMA clusters (SA trimers and tetramers) decline with increasing temperature, despite variations in precursor concentrations and CS across sites. For instance,~~The effect of temperature can also be reflected in larger clusters, like SA trimer and tetramer (Figure 2).~~ although TL exhibited higher $[SA_1]$ (~2.6×10^7 cm^{-3}) during high-temperature (~303 K) NPF periods, the abundance and diversity of measured clusters were lower than those at low-temperature sites (WD and DLW). Theoretically, the evaporation rates of SA trimers and tetramers show limited sensitivity to temperature (Olenius et al., 2017), and their variation can be even neglected in some cluster dynamics models (Cai et al., 2021). Thus, the observed reduction in larger clusters at elevated temperatures is likely constrained by the formation of SA_2. The proportion of base molecules in clusters also decreased with increasing temperature in the four selected NPF events, which was also reported in CLOUD experiments (Schobesberger et al., 2015). Furthermore, with the increase of cluster size, NH_3 tends to gradually replace DMA in ion clusters (Schobesberger et al., 2015; Yin et al., 2021), enhancing the stability of SA-base clusters (Bzdek et al., 2017), which helps them resist evaporation.~~Even though the high-temperature (303 K) NPF period at TL had the higher $[SA_1]$ (~2.6×10^7 cm^{-3}), the abundance and variety of measured cluster were lower than those on low temperatures (275 K and 277 K) at WD and DLW. In addition to temperature, the effect of [DMA] on $[SA_2]$ was also described in Figure S4. The rise in [DMA] considerably promotes the generation of SA_2, the promotion efficiency is gradually not obvious meanwhile, because [DMA] is close to nucleation saturation (Almeida et al., 2013).~~

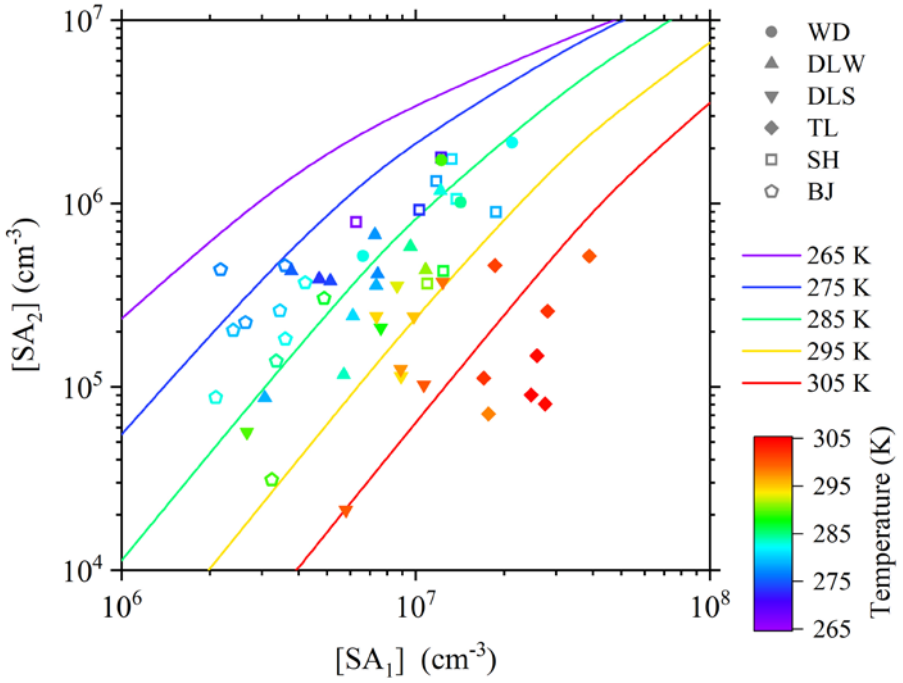

Figure 5: $[SA_2]_{scaled}$ as a function of $[SA_1]$ under a temperature gradient. Each symbol indicates one NPF event with a time resolution of 30 min, which was selected when $J_{1.7,meas}$ reaches maximum. [DMA] and CS for the simulated lines calculated by the discrete-sectional model are their median values in all NPF events, i.e., 0.017 s^{-1} and 2.3 pptv, respectively. To visualize the effect of temperature, the color of the simulated lines corresponds to the color bar.

As shown in Figure 6, the particle formation rate exhibits a negative correlation with temperature. Notably, for a fixed $[SA_1]$, the formation rate varies by~~The significant effect of temperature on cluster stability further causes large differences in $J_{1.4}$ (Figure 6). Specifically, the values of scaled $J_{1.4}$ ($J_{1.4,scaled}$) span~~ approximately ~~3~~ three orders of magnitude ~~for the same $[SA_1]$~~ over a 30 K temperature range, and this extent of variation is comparable to that reported in chamber experiments simulating the conditions of polluted environments (Xiao et al., 2021) and atmospheric observations in urban area (Yu et al., 2016)~~ of about 30 K~~. This highlights the critical role of temperature in modulating nucleation, suggesting that temperature fluctuations alone can induce major~~lead to substantial~~ variability in NPF without the change in the species and concentrations~~major~~ nucleation precursors. In other words, SA and DMA can still explain the wide range of $J_{1.4,scaled}$ at these sites. The significant effect of temperature on cluster stability seems to further lead to substantial variations in $J_{1.4}$, since~~In terms of trends, $J_{1.4,scaled}$ exhibits a negative correlation with temperature, which is consistent with published atmospheric investigations (Yu et al., 2016; Deng et al., 2020). Similar to $[SA_2]$,~~ the evaporation rate of SA_1DMA_1 can be considered as ~~is~~ a key factor influencing the~~ temperature~~ dependence of particle formation rate on temperature (Deng et al., 2020~~; Cai et al., 2022b~~). ~~It is evident that the temperature dependence of $J_{1.4}$ was not as pronounced as that of SA_2, particularly data points at DL, which are clustered together with the temperature range of ~20 K. Some of them also correspond worse to the simulated results, compared with data points in other campaigns. The temperature dependence of $J_{1.4}$ at DL was obvious in the inter-comparison of each campaign (Figure S5), when all campaigns collectively analyzed, the presentation of temperature dependence is subject to systematic uncertainties across different campaigns.~~

In the analyses presented above, temperature is regarded as a dominant factor determining the intensity of NPF over large regional scales. The direct effect of temperature on NPF is negative, through altering the evaporation rates of clusters (Olenius et al., 2017; Myllys et al., 2019). This has been consistently demonstrated in well-controlled chamber experiments with different nucleation mechanisms (Kirkby et al., 2011; Simon et al., 2020; Xiao et al., 2021; He et al., 2023). When temperature differences are substantial, its inhibitory effect on NPF becomes evident in complex ambient environments. For example, Baalbaki et al. (2021) reported the particle formation rate in warmer months was actually lower than that in cooler months with comparable $[SA_1]$ levels in the Eastern Mediterranean. Inter-site comparisons in India showed a negative correlation

between particle formation rate and temperature, although precursor concentrations were not measured (Kanawade et al., 2022). However, under conditions of limited temperature variability, the effect of temperature is less directly observable, and higher temperatures may even appear to favor NPF (Größ et al., 2018; Brean et al., 2020; Yan et al., 2021; Victor et al., 2024). This may stem from other temperature-related factors. For example, in atmospheric observations, temperature is often correlated positively with solar radiation, which directly promotes the formation of nucleation precursors (Kürten et al., 2016; Brean et al., 2020). Additionally, temperature is typically negatively correlated with relative humidity, and high humidity suppresses NPF via hygroscopic growth of pre-existing particles (Määttänen et al., 2018).

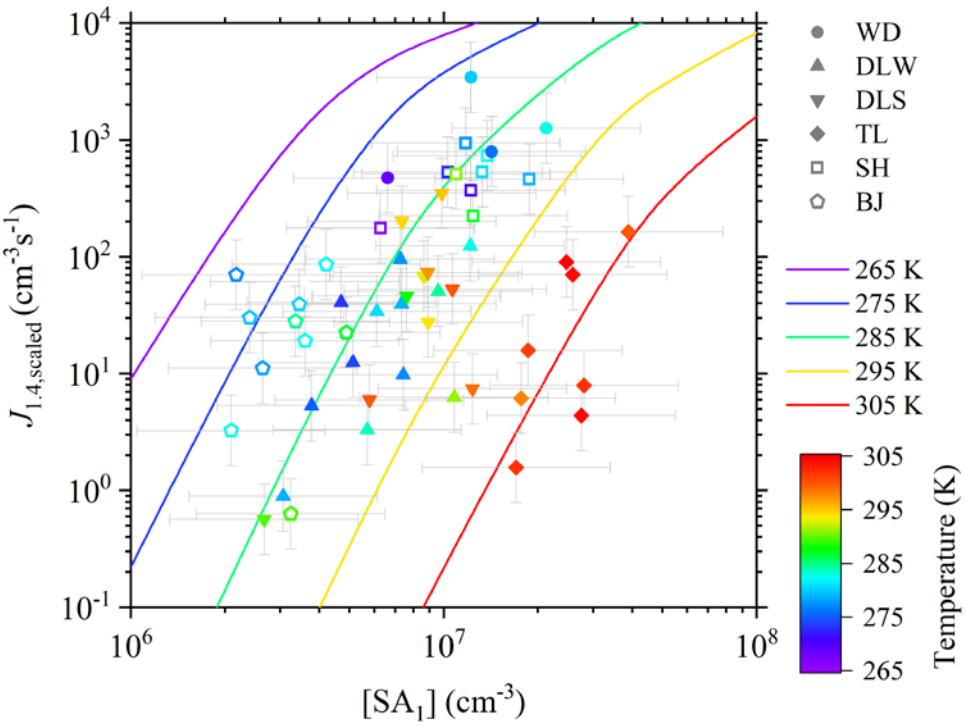

Figure 6: $J_{1.4,scaled}$ as a function of [SA_1] under the temperature gradient. Each symbol indicates one NPF events with a time resolution of 30 min, which were selected when $J_{1.7,meas}$ reaches maximum. [DMA] and CS for the simulated lines by the discrete-sectional model are their median values in all NPF events, i.e., 0.017 s^{-1} and 2.3 pptv, respectively. Horizontal and vertical error bars connected with each symbol indicate the uncertainties of x-axis and y-axis, respectively. To visualize the effect of temperature, the color of the simulated lines corresponds to the color bar.

3.~~3~~ 4 Initial growth of nucleated particles

The ~~discussions~~ analyze above ~~have~~ has shown that SA~~-~~ and DMA can explain atmospheric nucleation ~~could explain predominant nucleation mechanism at five sites~~. Here, ~~we investigate~~ the ~~contribution of particle~~ initial growth of nucleated particles is investigated~~to $J_{1.7}$~~. Figure 7a ~~presents~~ compares the ~~comparison of~~ simulated growth rate of 1.4-1.7 nm particles ($GR_{1.4\text{-}1.7}$) with two ~~groups~~ sets of condensable vapors at BJ and DLS. When only SA and its clusters are included, the simulated~~the contribution of sulfuric acid is considered, the~~ $GR_{1.4\text{-}1.7}$ ~~values~~ ranges ~~at the two sites range~~ approximately from 0.3 to 3.4 nm/h. ~~If $GR_{1.4\text{-}1.7}$ could be roughly approximated to growth rate of under 3 nm particles, these values of simulated $GR_{1.4\text{-}1.7}$ are in accordance with the measured range (0.5-14.3 nm/h) in previous reports from the eastern region of China (Xiao et al., 2015; Dai et al., 2017; Yao et al., 2018; Hong et al., 2023).~~ The simulated $GR_{1.4\text{-}1.7}$ is enhanced when OOMs are also considered as condensable vapors on the basis of the contribution of SA and its clusters, ranging approximately from 1.2 to 22.6 nm/h. Assuming $GR_{1.4\text{-}1.7}$ is roughly approximated to the growth rate of sub-3 nm particles, these simulated values are

generally in accordance with the measured range (0.5-20.4 nm/h) in previous reports from the eastern region of China (Xiao et al., 2015; Dai et al., 2017; Yao et al., 2018; Hong et al., 2023). The corresponding simulation results from the other four campaigns are generally consistent with those at BJ and DLS, differing mainly in the extent of growth rate enhancement (Figure S8a).~~. The same comparison in other four campaigns is shown in Figure S6a.The volatility distribution of observed OOMs for simulating is shown in Figure S7. Here, it is assumed that only SA, its clusters and OOMs contribute to $GR_{1.4-1.7}$, because they can largely explain the growth of particles in urban areas (Qiao et al., 2021).~~

The comparison between $J_{1.7,meas}$ and simulated $J_{1.7}$ ($J_{1.7,sim}$) provides support for the contribution of OOMs to the growth of nucleated particles (Figure 7b).~~The simulation of $J_{1.7}$ is improved by considering the contribution of OOMs to the initial growth of new particles. The comparison between $J_{1.7,meas}$ and the simulated $J_{1.7}$ ($J_{1.7,sim}$) at BJ and DLS is shown in Figure 7b.~~ When ~~merely~~ only~~considering the contribution of~~ SA and its clusters are considered, a substantial deviation, sometimes more than three orders of magnitude, is observed~~to GR, there is a significant deviation~~ between~~ the values of~~ $J_{1.7,meas}$ and $J_{1.7,sim}$ ~~generally, and some of them even deviated by more than 3 orders of magnitude~~. Compared to the simulation of $J_{1.4}$ (Figure ~~S2~~S7), $J_{1.7,sim}$ shows a noticeable decline ~~the values of $J_{1.7,sim}$~~ at DLS and BJ. The inclusion of OOM-induced growth markedly increases $J_{1.7,sim}$, leading to better agreements with measurements, which can also be supported by observations in CLOUD experiments (Tröstl et al., 2016).~~also reveal an evident decline. After incorporating the contribution of OOMs to $GR_{1.4-1.7}$, the values of $J_{1.7,sim}$ are greatly elevated.~~ The corresponding ~~results of~~ improvement are limited~~poor~~ at WD, DLW, TL and SH, where the contribution of SA and its clusters seems sufficient to explain $GR_{1.4-1.7}$ (Figure S8b).~~and the contribution of SA and its clusters seems sufficient to explain $GR_{1.4-1.7}$ in these campaigns (Figure S6b).~~ In fact, ~~OOMs may also be involved in clustering, especially at DL and TL with high concentrations of~~some ultralow volatile organic compounds within OOMs may be involved in~~(Figure S7), which are capable of~~ nucleating (Simon et al., 2020). Nevertheless, even without considering their contribution in this stage, the condensation of OOMs exerts a considerable influence on initial growth, as reflected in $J_{1.7}$. Moreover, $J_{1.7}$ exhibits strong temperature dependence, similar to $J_{1.4}$ (Figure S9).~~regardless of their contribution to nucleation, their effects on condensation were also considerable to $J_{1.7}$, which also demonstrates strong temperature dependence like $J_{1.4}$ (Figure S8).~~

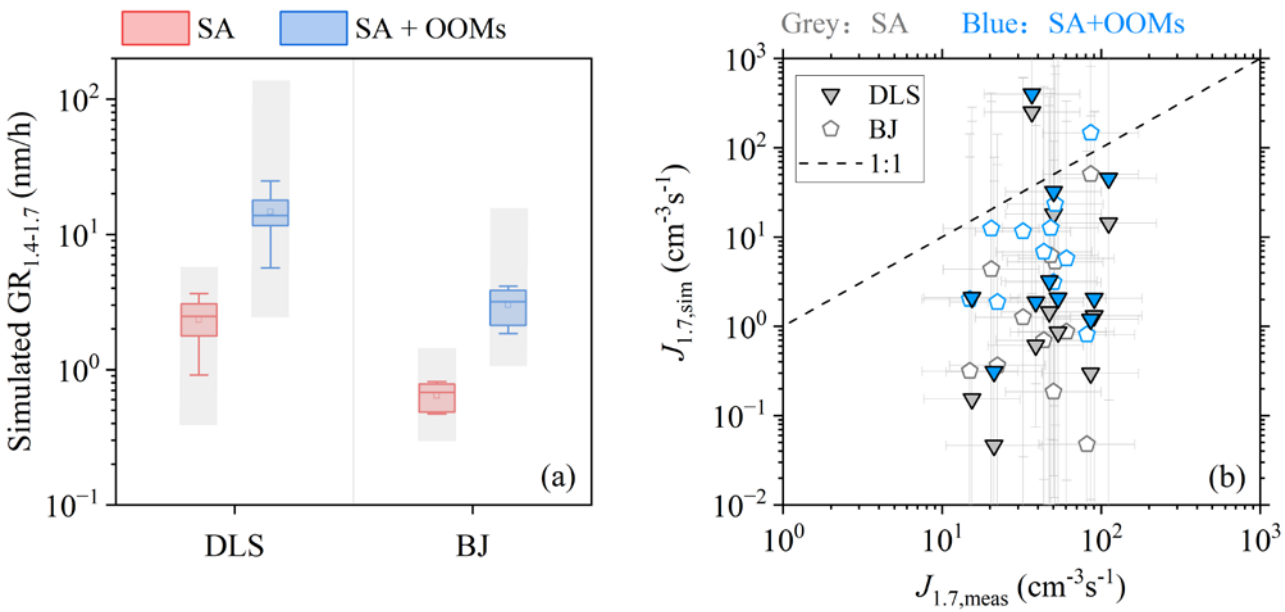

Figure 7: The simulation of $GR_{1.4-1.7}$ and $J_{1.7}$. (a) The comparison of simulated $GR_{1.4-1.7}$ contributed by SA and its clusters (i.e. SA in the legend), as well as SA and its clusters plus OOMs in campaigns. The transverse lines and square markers inside the boxes indicate mean values and median values, respectively. The bottom and top edges of the box indicate the 25th and 75th percentiles, respectively. The bottom and top edges of the whisker lines outside of the boxes indicate the 10th and 90th percentiles, respectively. The shade boxes indicate the ranges of uncertainties. (b)The comparison between $J_{1.7,meas}$ and $J_{1.7,sim}$. Horizontal and vertical error bars connected with each symbol indicate the uncertainties of x-axis and y-axis, respectively.

4 Conclusions

We studied the mechanism and influencing factors of NPF on a large spatial scale by using observational data at multiple sites in the eastern region of China,~~We analyze the governing mechanism SA-DMA in the eastern region of China using observation data at three sites,~~ including the concentrations of key chemical species, ~~meteorological parameters~~temperature and PSD.

By Comparing with previous studies that investigated atmospheric nucleation mechanism in individual sites, we have showed the applicability of a similar mechanism over a large geographic region. Based on the correlation between [SA_1] and particle formation rate, the identification of key clusters, and comparisons between simulations and measurements, we concluded that nucleating processes~~Both the nucleating clusters~~, mainly exemplified by SA_2~~,~~ and ~~the nucleation rates, represented by~~ $J_{1.4}$, ~~can~~ could be largely attributed to~~ the collisions between~~ SA~~ and~~ DMA collision~~to a large extent.~~, although other precursors, such as NH_3 and OOMs, might also participated. However, SA and its clusters ~~are~~ were insufficient, at least at DSL and BJ, to explain the initial growth of ~~freshly~~ nucleated particles, while OOMs make great contribution to this process, thereby affecting $J_{1.7}$, which was derived from model-observation comparisons. While previous understanding of the contribution of OOMs to initial particle growth was reflected by chamber studies, our study provides supporting evidence from atmospheric observations.~~.~~ Given the considerable spatial separation among ~~the~~ five sites, ~~it is thus~~we infer~~red~~ that within this extensive urban agglomeration~~geographical scope~~, SA and DMA are capable of describing atmospheric nucleation up to 1.4 nm, whereas OOMs are potentially involved in in subsequent growth.~~$GR_{1.4-1.7}$, thereby improving the simulation performance of $J_{1.7}$, which is derived from model-observation comparisons, and direct experimental evidence remains to be substantiated.~~ This may also apply to other populated and polluted regions, where the NPF mechanism warrants investigation.~~Besides, the effect of temperature on SA-DMA nucleation was illustrated quantitatively through scaling, and the differences in nucleation intensity among campaigns could also be demonstrated by variations in temperature under the same mechanism. With the notable reduction in [SO_2] and [amines] in recent years (Liu et al., 2023; Du et al., 2025), and the strong dependence of [SO_2] on [SA_1] production (Lu et al., 2019), the applicability of SA-DMA mechanism to atmospheric nucleation over a wide spatial scale in the eastern region of China, as well as other densely populated and polluted regions may continually evolve, which warrants further investigation in the future.~~

As for influencing factors, the occurrence of NPF was governed by [SA_1] and CS, whereas the frequency and intensity of NPF were mainly determined by temperature, which generally exhibited a negative correlation with NPF over a wide temperature range. Compared with previous studies investigating NPF dependence on temperature from a temporal perspective, dependences of cluster concentrations and particle formation rates on temperature were illustrated quantitatively through scaling at five sites, suggesting the differences in nucleation intensity across this region could be explained by variations in temperature under the comparable mechanism. We expect that this finding holds for similar polluted atmospheric environments on large spatial scales worldwide, particularly where significant temperature gradients exist.

The case for SA-DMA nucleation presented in this study remains indirect, as it relies on precursors, limited clusters and modeling rather than comprehensive identification of nucleation process. To better resolve atmospheric nucleation mechanisms, future studies are warranted to advance beyond current methods of cluster detection, for instance, by enabling direct measurements of all basic molecules within SA clusters. In the complex urban atmosphere, the potential involvement of other pollutants will require novel direct measurements and analytical techniques, along with more comprehensive modeling, to clarify the roles of additional precursors.

References

Alfaouri, D., Passananti, M., Zanca, T., Ahonen, L., Kangasluoma, J., Kubečka, J., Myllys, N., and Vehkamäki, H.: A study on the fragmentation of sulfuric acid and dimethylamine clusters inside an atmospheric pressure interface time-of-flight mass

spectrometer, Atmos. Meas. Tech., 15, 11–19, https://doi.org/10.5194/amt-15-11-2022, 2022.

Almeida, J., Schobesberger, S., Kuerten, A., Ortega, I. K., Kupiainen-Maatta, O., Praplan, A. P., Adamov, A., Amorim, A., Bianchi, F., Breitenlechner, M., David, A., Dommen, J., Donahue, N. M., Downard, A., Dunne, E., Duplissy, J., Ehrhart, S., Flagan, R. C., Franchin, A., Guida, R., Hakala, J., Hansel, A., Heinritzi, M., Henschel, H., Jokinen, T., Junninen, H., Kajos, M., Kangasluoma, J., Keskinen, H., Kupc, A., Kurten, T., Kvashin, A. N., Laaksonen, A., Lehtipalo, K., Leiminger, M., Leppa, J., Loukonen, V., Makhmutov, V., Mathot, S., McGrath, M. J., Nieminen, T., Olenius, T., Onnela, A., Petaja, T., Riccobono, F., Riipinen, I., Rissanen, M., Rondo, L., Ruuskanen, T., Santos, F. D., Sarnela, N., Schallhart, S., Schnitzhofer, R., Seinfeld, J. H., Simon, M., Sipila, M., Stozhkov, Y., Stratmann, F., Tome, A., Troestl, J., Tsagkogeorgas, G., Vaattovaara, P., Viisanen, Y., Virtanen, A., Vrtala, A., Wagner, P. E., Weingartner, E., Wex, H., Williamson, C., Wimmer, D., Ye, P., Yli-Juuti, T., Carslaw, K. S., Kulmala, M., Curtius, J., Baltensperger, U., Worsnop, D. R., Vehkamaki, H., and Kirkby, J.: Molecular understanding of sulphuric acid-amine particle nucleation in the atmosphere, Nature, 502, 359–363, https://doi.org/10.1038/nature12663, 2013.

Baalbaki, R., Pikridas, M., Jokinen, T., Laurila, T., Dada, L., Bezantakos, S., Ahonen, L., Neitola, K., Maisser, A., Bimenyimana, E., Christodoulou, A., Unga, F., Savvides, C., Lehtipalo, K., Kangasluoma, J., Biskos, G., Petäjä, T., Kerminen, V.-M., Sciare, J., and Kulmala, M.: Towards understanding the characteristics of new particle formation in the Eastern Mediterranean, Atmos. Chem. Phys., 21, 9223–9251, https://doi.org/10.5194/acp-21-9223-2021, 2021.

Bianchi, F., Tröstl, J., Junninen, H., Frege, C., Henne, S., Hoyle, C. R., Molteni, U., Herrmann, E., Adamov, A., Bukowiecki, N., Chen, X., Duplissy, J., Gysel, M., Hutterli, M., Kangasluoma, J., Kontkanen, J., Kürten, A., Manninen, H. E., Münch, S., Peräkylä, O., Petäjä, T., Rondo, L., Williamson, C., Weingartner, E., Curtius, J., Worsnop, D. R., Kulmala, M., Dommen, J., and Baltensperger, U.: New particle formation in the free troposphere: A question of chemistry and timing, Science, 352, 1109–1112, https://doi.org/10.1126/science.aad5456, 2016.

Bousiotis, D., Pope, F. D., Beddows, D. C. S., Dall'Osto, M., Massling, A., Nojgaard, J. K., Nordstrom, C., Niemi, J. V., Portin, H., Petaja, T., Perez, N., Alastuey, A., Querol, X., Kouvarakis, G., Mihalopoulos, N., Vratolis, S., Eleftheriadis, K., Wiedensohler, A., Weinhold, K., Merkel, M., Tuch, T., and Harrison, R. M.: A phenomenology of new particle formation (NPF) at 13 European sites, Atmos. Chem. Phys., 21, 11905–11925, https://doi.org/10.5194/acp-21-11905-2021, 2021.

Brean, J., Beddows, D. C. S., Shi, Z., Temime-Roussel, B., Marchand, N., Querol, X., Alastuey, A., Minguillon, M. C., and Harrison, R. M.: Molecular insights into new particle formation in Barcelona, Spain, Atmos. Chem. Phys., 20, 10029–10045, https://doi.org/10.5194/acp-20-10029-2020, 2020.

Bzdek, B. R., DePalma, J. W., and Johnston, M. V.: Mechanisms of atmospherically relevant cluster growth, Acc. Chem. Res., 50, 1965–1975, https://doi.org/10.1021/acs.accounts.7b00213, 2017.

Cai, J., Sulo, J., Gu, Y., Holm, S., Cai, R., Thomas, S., Neuberger, A., Mattsson, F., Paglione, M., Decesari, S., Rinaldi, M., Yin, R., Aliaga, D., Huang, W., Li, Y., Gramlich, Y., Ciarelli, G., Quéléver, L., Sarnela, N., Lehtipalo, K., Zannoni, N., Wu, C., Nie, W., Kangasluoma, J., Mohr, C., Kulmala, M., Zha, Q., Stolzenburg, D., and Bianchi, F.: Elucidating the mechanisms of atmospheric new particle formation in the highly polluted Po Valley, Italy, Atmos. Chem. Phys., 24, 2423–2441, https://doi.org/10.5194/acp-24-2423-2024, 2024.

Cai, R., Yan, C., Yang, D., Yin, R., Lu, Y., Deng, C., Fu, Y., Ruan, J., Li, X., Kontkanen, J., Zhang, Q., Kangasluoma, J., Ma, Y., Hao, J., Worsnop, D. R., Bianchi, F., Paasonen, P., Kerminen, V.-M., Liu, Y., Wang, L., Zheng, J., Kulmala, M., and Jiang, J.: Sulfuric acid-amine nucleation in urban Beijing, Atmos. Chem. Phys., 21, 2457–2468, https://doi.org/10.5194/acp-21-2457-2021, 2021.

Cai, R., Deng, C., Stolzenburg, D., Li, C., Guo, J., Kerminen, V.-M., Jiang, J., Kulmala, M., and Kangasluoma, J.: Survival probability of new atmospheric particles: closure between theory and measurements from 1.4 to 100 nm, Atmos. Chem. Phys., 22, 14571–14587, https://doi.org/10.5194/acp-22-14571-2022, 2022a.

Cai, R., Yin, R., Yan, C., Yang, D., Deng, C., Dada, L., Kangasluoma, J., Kontkanen, J., Halonen, R., Ma, Y., Zhang, X., Paasonen, P., Petaja, T., Kerminen, V.-M., Liu, Y., Bianchi, F., Zheng, J., Wang, L., Hao, J., Smith, J. N., Donahue, N. M., Kulmala, M., Worsnop, D. R., and Jiang, J.: The missing base molecules in atmospheric acid-base nucleation, Natl. Sci. Rev., 9, nwac137, https://doi.org/10.1093/nsr/nwac137, 2022b.

Chang, Y., Gao, Y., Lu, Y., Qiao, L., Kuang, Y., Cheng, K., Wu, Y., Lou, S., Jing, S., Wang, H., and Huang, C.: Discovery of a

potent source of gaseous amines in urban China, Environ. Sci. Technol. Lett., 8, 725–731, https://doi.org/10.1021/acs.estlett.1c00229, 2021.

Dai, L., Wang, H., Zhou, L., An, J., Tang, L., Lu, C., Yan, W., Liu, R., Kong, S., Chen, M., Lee, S., and Yu, H.: Regional and local new particle formation events observed in the Yangtze River Delta region, China, J. Geophys. Res.-Atmos., 122, 2389–2402, https://doi.org/10.1002/2016JD026030, 2017.

Deng, C., Fu, Y., Dada, L., Yan, C., Cai, R., Yang, D., Zhou, Y., Yin, R., Lu, Y., Li, X., Qiao, X., Fan, X., Nie, W., Kontkanen, J., Kangasluoma, J., Chu, B., Ding, A., Kerminen, V.-M., Paasonen, P., Worsnop, D. R., Bianchi, F., Liu, Y., Zheng, J., Wang, L., Kulmala, M., and Jiang, J.: Seasonal characteristics of new particle formation and growth in urban Beijing, Environ. Sci. Technol., 54, 8547–8557, https://doi.org/10.1021/acs.est.0c00808, 2020.

~~Deng, K., Huo, J., Wang, Y., Wang, L., Yin, S., Li, C., Li, Y., Yang, G., Yao, L., Fu, Q., and Wang, L.: Characteristics of atmospheric reduced sulfur compounds at a suburban site of Shanghai, J. Environ. Sci., 156, 671–683, https://doi.org/10.1016/j.jes.2024.06.030, 2025.~~

Dinoi, A., Gulli, D., Weinhold, K., Ammoscato, I., Calidonna, C. R., Wiedensohler, A., and Contini, D.: Characterization of ultrafine particles and the occurrence of new particle formation events in an urban and coastal site of the Mediterranean area, Atmos. Chem. Phys., 23, 2167–2181, https://doi.org/10.5194/acp-23-2167-2023, 2023.

~~Du, W., Jiang, S., Fu, N., Song, J., Lin, X., Mao, K., Shi, J., Chen, Y., Liu, J., and Tao, S.: Ammonia and amines emissions from residential biomass combustion in China from 2014 to 2030, J. Hazard. Mater., 488, 137476, https://doi.org/10.1016/j.jhazmat.2025.137476, 2025.~~

Freshour, N. A., Carlson, K. K., Melka, Y. A., Hinz, S., Panta, B., and Hanson, D. R.: Amine permeation sources characterized with acid neutralization and sensitivities of an amine mass spectrometer, Atmos. Meas. Tech., 7, 3611–3621, https://doi.org/10.5194/amt-7-3611-2014, 2014.

Gordon, H., Kirkby, J., Baltensperger, U., Bianchi, F., Breitenlechner, M., Curtius, J., Dias, A., Dommen, J., Donahue, N. M., Dunne, E. M., Duplissy, J., Ehrhart, S., Flagan, R. C., Frege, C., Fuchs, C., Hansel, A., Hoyle, C. R., Kulmala, M., Kurten, A., Lehtipalo, K., Makhmutov, V., Molteni, U., Rissanen, M. P., Stozkhov, Y., Trostl, J., Tsagkogeorgas, G., Wagner, R., Williamson, C., Wimmer, D., Winkler, P. M., Yan, C., and Carslaw, K. S.: Causes and importance of new particle formation in the present-day and preindustrial atmospheres, J. Geophys. Res.-Atmos., 122, 8739–8760, https://doi.org/10.1002/2017JD026844, 2017.

Größ, J., Hamed, A., Sonntag, A., Spindler, G., Manninen, H. E., Nieminen, T., Kulmala, M., Hõrrak, U., Plass-Dülmer, C., Wiedensohler, A., and Birmili, W.: Atmospheric new particle formation at the research station Melpitz, Germany: connection with gaseous precursors and meteorological parameters, Atmos. Chem. Phys., 18, 1835–1861, https://doi.org/10.5194/acp-18-1835-2018, 2018.

Hanson, D. R., McMurry, P. H., Jiang, J., Tanner, D., and Huey, L. G.: Ambient pressure proton transfer mass spectrometry: detection of amines and ammonia, Environ. Sci. Technol., 45, 8881–8888, https://doi.org/10.1021/es201819a, 2011.

He, X.-C., Simon, M., Iyer, S., Xie, H.-B., Roerup, B., Shen, J., Finkenzeller, H., Stolzenburg, D., Zhang, R., Baccarini, A., Tham, Y. J., Wang, M., Amanatidis, S., Piedehierro, A. A., Amorim, A., Baalbaki, R., Brasseur, Z., Caudillo, L., Chu, B., Dada, L., Duplissy, J., El Haddad, I., Flagan, R. C., Granzin, M., Hansel, A., Heinritzi, M., Hofbauer, V., Jokinen, T., Kemppainen, D., Kong, W., Krechmer, J., Kuerten, A., Lamkaddam, H., Lopez, B., Ma, F., Mahfouz, N. G. A., Makhmutov, V., Manninen, H. E., Marie, G., Marten, R., Massabo, D., Mauldin, R. L., Mentler, B., Onnela, A., Petaejae, T., Pfeifer, J., Philippov, M., Ranjithkumar, A., Rissanen, M. P., Schobesberger, S., Scholz, W., Schulze, B., Surdu, M., Thakur, R. C., Tome, A., Wagner, A. C., Wang, D., Wang, Y., Weber, S. K., Welti, A., Winkler, P. M., Zauner-Wieczorek, M., Baltensperger, U., Curtius, J., Kurten, T., Worsnop, D. R., Volkamer, R., Lehtipalo, K., Kirkby, J., Donahue, N. M., Sipilae, M., and Kulmala, M.: Iodine oxoacids enhance nucleation of sulfuric acid particles in the atmosphere, Science, 382, 1308–1314 https://doi.org/10.1126/science.adh2526, 2023.

Heinritzi, M., Simon, M., Steiner, G., Wagner, A. C., Kürten, A., Hansel, A., and Curtius, J.: Characterization of the mass-dependent transmission efficiency of a CIMS, Atmos. Meas. Tech., 9, 1449–1460, https://doi.org/10.5194/amt-9-1449-2016, 2016.

Hong, J., Tang, M., Wang, Q., Ma, N., Zhu, S., Zhang, S., Pan, X., Xie, L., Li, G., Kuhn, U., Yan, C., Tao, J., Kuang, Y., He,

Y., Xu, W., Cai, R., Zhou, Y., Wang, Z., Zhou, G., Yuan, B., Cheng, Y., and Su, H.: Measurement report: Wintertime new particle formation in the rural area of the North China Plain - influencing factors and possible formation mechanism, Atmos. Chem. Phys., 23, 5699–5713, https://doi.org/10.5194/acp-23-5699-2023, 2023.

~~Hu, X., Yang, G., Liu, Y., Lu, Y., Wang, Y., Chen, H., Chen, J., and Wang, L.: Atmospheric gaseous organic acids in winter in a rural site of the North China Plain, J. Environ. Sci., 113, 190–203, https://doi.org/10.1016/j.jes.2021.05.035, 2022.~~Jen, C. N., McMurry, P. H., and Hanson, D. R.: Stabilization of sulfuric acid dimers by ammonia, methylamine, dimethylamine, and trimethylamine, J. Geophys. Res.-Atmos, 119, 7502–7514, https://doi.org/10.1002/2014JD021592, 2014.

Kanawade, V. P., Sebastian, M., Hooda, R. K., and Hyvärinen, A.-P.: Atmospheric new particle formation in India: Current understanding and knowledge gaps, Atmos. Environ., 270, 118894, https://doi.org/10.1016/j.atmosenv.2021.118894, 2022.

Kerminen, V.-M., Chen, X., Vakkari, V., Petaja, T., Kulmala, M., and Bianchi, F.: Atmospheric new particle formation and growth: review of field observations, Environ. Res. Lett., 13, 103003, https://doi.org/10.1088/1748-9326/aadf3c, 2018.

Kirkby, J., Curtius, J., Almeida, J., Dunne, E., Duplissy, J., Ehrhart, S., Franchin, A., Gagne, S., Ickes, L., Kuerten, A., Kupc, A., Metzger, A., Riccobono, F., Rondo, L., Schobesberger, S., Tsagkogeorgas, G., Wimmer, D., Amorim, A., Bianchi, F., Breitenlechner, M., David, A., Dommen, J., Downard, A., Ehn, M., Flagan, R. C., Haider, S., Hansel, A., Hauser, D., Jud, W., Junninen, H., Kreissl, F., Kvashin, A., Laaksonen, A., Lehtipalo, K., Lima, J., Lovejoy, E. R., Makhmutov, V., Mathot, S., Mikkila, J., Minginette, P., Mogo, S., Nieminen, T., Onnela, A., Pereira, P., Petaja, T., Schnitzhofer, R., Seinfeld, J. H., Sipila, M., Stozhkov, Y., Stratmann, F., Tome, A., Vanhanen, J., Viisanen, Y., Vrtala, A., Wagner, P. E., Walther, H., Weingartner, E., Wex, H., Winkler, P. M., Carslaw, K. S., Worsnop, D. R., Baltensperger, U., and Kulmala, M.: Role of sulphuric acid, ammonia and galactic cosmic rays in atmospheric aerosol nucleation, Nature, 476, 429-433, https://doi.org/10.1038/nature10343, 2011.

Kirkby, J., Amorim, A., Baltensperger, U., Carslaw, K. S., Christoudias, T., Curtius, J., Donahue, N. M., Haddad, I. E., Flagan, R. C., Gordon, H., Hansel, A., Harder, H., Junninen, H., Kulmala, M., Kürten, A., Laaksonen, A., Lehtipalo, K., Lelieveld, J., Möhler, O., Riipinen, I., Stratmann, F., Tomé, A., Virtanen, A., Volkamer, R., Winkler, P. M., and Worsnop, D. R.: Atmospheric new particle formation from the CERN CLOUD experiment, Nat. Geosci., 16, 948–957, https://doi.org/10.1038/s41561-023-01305-0, 2023.

~~Kulmala, M., Kokkonen, T., Pekkanen, J., Paatero, S., Petaja, T., Kerminen, V. M., and Ding, A.: Opinion: Gigacity – a source of problems or the new way to sustainable development, Atmos. Chem. Phys., 21, 8313–8322, https://doi.org/10.5194/acp-21-8313-2021, 2021.~~

Kürten, A., Jokinen, T., Simon, M., Sipilä, M., Sarnela, N., Junninen, H., Adamov, A., Almeida, J., Amorim, A., Bianchi, F., Breitenlechner, M., Dommen, J., Donahue, N. M., Duplissy, J., Ehrhart, S., Flagan, R. C., Franchin, A., Hakala, J., Hansel, A., Heinritzi, M., Hutterli, M., Kangasluoma, J., Kirkby, J., Laaksonen, A., Lehtipalo, K., Leiminger, M., Makhmutov, V., Mathot, S., Onnela, A., Petäjä, T., Praplan, A. P., Riccobono, F., Rissanen, M. P., Rondo, L., Schobesberger, S., Seinfeld, J. H., Steiner, G., Tomé, A., Tröstl, J., Winkler, P. M., Williamson, C., Wimmer, D., Ye, P., Baltensperger, U., Carslaw, K. S., Kulmala, M., Worsnop, D. R., and Curtius, J.: Neutral molecular cluster formation of sulfuric acid–dimethylamine observed in real time under atmospheric conditions, Proc. Natl. Acad. Sci. U. S. A., 111, 15019–15024, https://doi.org/10.1073/pnas.1404853111, 2014.

Kürten, A., Bergen, A., Heinritzi, M., Leiminger, M., Lorenz, V., Piel, F., Simon, M., Sitals, R., Wagner, A. C., and Curtius, J.: Observation of new particle formation and measurement of sulfuric acid, ammonia, amines and highly oxidized organic molecules at a rural site in central Germany, Atmos. Chem. Phys., 16, 12793–12813, https://doi.org/10.5194/acp-16-12793-2016, 2016.

Kürten, A., Li, C., Bianchi, F., Curtius, J., Dias, A., Donahue, N. M., Duplissy, J., Flagan, R. C., Hakala, J., Jokinen, T., Kirkby, J., Kulmala, M., Laaksonen, A., Lehtipalo, K., Makhmutov, V., Onnela, A., Rissanen, M. P., Simon, M., Sipilä, M., Stozhkov, Y., Tröstl, J., Ye, P., and McMurry, P. H.: New particle formation in the sulfuric acid–dimethylamine–water system: reevaluation of CLOUD chamber measurements and comparison to an aerosol nucleation and growth model, Atmos. Chem. Phys., 18, 845–863, https://doi.org/10.5194/acp-18-845-2018, 2018.

Larriba, C., Hogan Jr., C. J., Attoui, M., Borrajo, R., Garcia, J. F., and de la Mora, J. F.: The mobility–volume relationship below 3.0 nm examined by tandem mobility–mass measurement, Aerosol Sci. Tech., 45, 453–467, https://doi.org/10.1080/02786826.2010.546820, 2011.

Lee, H., Cho, H., Yoon, Y. J., Kim, J., Lee, B. Y., and Park, K.: Comparison of new particle formation events in urban, agricultural, and arctic environments, Atmos. Environ., 333, 120634, https://doi.org/10.1016/j.atmosenv.2024.120634, 2024.

Li, C., Li, Y., Li, X., Cai, R., Fan, Y., Qiao, X., Yin, R., Yan, C., Guo, Y., Liu, Y., Zheng, J., Kerminen, V.-M., Kulmala, M., Xiao, H., and Jiang, J.: Comprehensive simulations of new particle formation events in Beijing with a cluster dynamics-multicomponent sectional model, Atmos. Chem. Phys., 23, 6879–6896, https://doi.org/10.5194/acp-23-6879-2023, 2023.

~~Liu, C., Lyu, W., Zhao, W., Zheng, F., and Lu, J.: Exploratory research on influential factors of China's sulfur dioxide emission based on symbolic regression, Environ. Monit. Assess., 195, 41, https://doi.org/10.1007/s10661-022-10595-7, 2023.~~

Lu, Y., Yan, C., Fu, Y., Chen, Y., Liu, Y., Yang, G., Wang, Y., Bianchi, F., Chu, B., Zhou, Y., Yin, R., Baalbaki, R., Garmash, O., Deng, C., Wang, W., Liu, Y., Petaja, T., Kerminen, V.-M., Jiang, J., Kulmala, M., and Wang, L.: A proxy for atmospheric daytime gaseous sulfuric acid concentration in urban Beijing, Atmos. Chem. Phys., 19, 1971–1983, https://doi.org/10.5194/acp-19-1971-2019, 2019.

~~Lu, Y., Liu, L., Ning, A., Yang, G., Liu, Y., Kurten, T., Vehkamaki, H., Zhang, X., and Wang, L.: Atmospheric sulfuric acid-dimethylamine nucleation enhanced by trifluoroacetic acid, Geophys. Res. Lett., 47, e2019GL085627, https://doi.org/10.1029/2019GL085627, 2020.~~

Määttänen, A., Merikanto, J., Henschel, H., Duplissy, J., Makkonen, R., Ortega, I. K., and Vehkamaki, H.: New Parameterizations for neutral and ion-induced sulfuric acid-water particle formation in nucleation and kinetic regimes, J. Geophys. Res.-Atmos., 123, 1269–1296, https://doi.org/10.1002/2017JD027429, 2018.

Mohr, C., Thornton, J. A., Heitto, A., Lopez-Hilfiker, F. D., Lutz, A., Riipinen, I., Hong, J., Donahue, N. M., Hallquist, M., Petäjä, T., Kulmala, M., and Yli-Juuti, T.: Molecular identification of organic vapors driving atmospheric nanoparticle growth, Nat. Commun., 10, 4442, https://doi.org/10.1038/s41467-019-12473-2, 2019.

Myllys, N., Kubečka, J., Besel, V., Alfaouri, D., Olenius, T., Smith, J. N., and Passananti, M.: Role of base strength, cluster structure and charge in sulfuric-acid-driven particle formation, Atmos. Chem. Phys., 19, 9753–9768, https://doi.org/10.5194/acp-19-9753-2019, 2019.

Nieminen, T., Kerminen, V.-M., Petäjä, T., Aalto, P. P., Arshinov, M., Asmi, E., Baltensperger, U., Beddows, D. C. S., Beukes, J. P., Collins, D., Ding, A., Harrison, R. M., Henzing, B., Hooda, R., Hu, M., Hõrrak, U., Kivekäs, N., Komsaare, K., Krejci, R., Kristensson, A., Laakso, L., Laaksonen, A., Leaitch, W. R., Lihavainen, H., Mihalopoulos, N., Németh, Z., Nie, W., O'Dowd, C., Salma, I., Sellegri, K., Svenningsson, B., Swietlicki, E., Tunved, P., Ulevicius, V., Vakkari, V., Vana, M., Wiedensohler, A., Wu, Z., Virtanen, A., and Kulmala, M.: Global analysis of continental boundary layer new particle formation based on long-term measurements, Atmos. Chem. Phys., 18, 14737–14756, https://doi.org/10.5194/acp-18-14737-2018, 2018.

Olenius, T., Halonen, R., Kurten, T., Henschel, H., Kupiainen-Maata, O., Ortega, I. K., Jen, C. N., Vehkamaki, H., and Riipinen, I.: New particle formation from sulfuric acid and amines: Comparison of monomethylamine, dimethylamine, and trimethylamine, J. Geophys. Res.-Atmos., 122, 7103–7118, https://doi.org/10.1002/2017JD026501, 2017.

~~Ortega, I. K., Kupiainen, O., Kurtén, T., Olenius, T., Wilkman, O., McGrath, M. J., Loukonen, V., and Vehkamäki, H.: From quantum chemical formation free energies to evaporation rates, Atmos. Chem. Phys., 12, 225–235, https://doi.org/10.5194/acp-12-225-2012, 2012.~~

Qiao, X., Yan, C., Li, X., Guo, Y., Yin, R., Deng, C., Li, C., Nie, W., Wang, M., Cai, R., Huang, D., Wang, Z., Yao, L., Worsnop, D. R., Bianchi, F., Liu, Y., Donahue, N. M., Kulmala, M., and Jiang, J.: Contribution of atmospheric oxygenated organic compounds to particle growth in an urban environment, Environ. Sci. Technol., 55, 13646–13656, https://doi.org/10.1021/acs.est.1c02095, 2021.

~~Ren, S., Yao, L., Wang, Y., Yang, G., Liu, Y., Li, Y., Lu, Y., Wang, L., and Wang, L.: Volatility parameterization of ambient organic aerosols a a rural site of the North China Plain, Atmos. Chem. Phys., 22, 9283–9297, https://doi.org/10.5194/acp-22-9283-2022, 2022.~~

Riccobono, F., Schobesberger, S., Scott, C. E., Dommen, J., Ortega, I. K., Rondo, L., Almeida, J., Amorim, A., Bianchi, F., Breitenlechner, M., David, A., Downard, A., Dunne, E. M., Duplissy, J., Ehrhart, S., Flagan, R. C., Franchin, A., Hansel, A., Junninen, H., Kajos, M., Keskinen, H., Kupc, A., Kürten, A., Kvashin, A. N., Laaksonen, A., Lehtipalo, K., Makhmutov, V., Mathot, S., Nieminen, T., Onnela, A., Petäjä, T., Praplan, A. P., Santos, F. D., Schallhart, S., Seinfeld, J. H., Sipilä, M., Spracklen, D. V., Stozhkov, Y., Stratmann, F., Tomé, A., Tsagkogeorgas, G., Vaattovaara, P., Viisanen, Y., Vrtala, A., Wagner,

P. E., Weingartner, E., Wex, H., Wimmer, D., Carslaw, K. S., Curtius, J., Donahue, N. M., Kirkby, J., Kulmala, M., Worsnop, D. R., and Baltensperger, U.: Oxidation products of biogenic emissions contribute to nucleation of atmospheric particles, Science, 344, 717–721, https://doi.org/10.1126/science.1243527, 2014.

Rose, C., Sellegri, K., Velarde, F., Moreno, I., Ramonet, M., Weinhold, K., Krejci, R., Ginot, P., Andrade, M., Wiedensohler, A., and Laj, P.: Frequent nucleation events at the high altitude station of Chacaltaya (5240 m a.s.l.), Bolivia, Atmos. Environ., 102, 18–29, https://doi.org/10.1016/j.atmosenv.2014.11.015, 2015.

Schobesberger, S., Franchin, A., Bianchi, F., Rondo, L., Duplissy, J., Kürten, A., Ortega, I. K., Metzger, A., Schnitzhofer, R., Almeida, J., Amorim, A., Dommen, J., Dunne, E. M., Ehn, M., Gagné, S., Ickes, L., Junninen, H., Hansel, A., Kerminen, V.-M., Kirkby, J., Kupc, A., Laaksonen, A., Lehtipalo, K., Mathot, S., Onnela, A., Petäjä, T., Riccobono, F., Santos, F. D., Sipilä, M., Tomé, A., Tsagkogeorgas, G., Viisanen, Y., Wagner, P. E., Wimmer, D., Curtius, J., Donahue, N. M., Baltensperger, U., Kulmala, M., and Worsnop, D. R.: On the composition of ammonia–sulfuric-acid ion clusters during aerosol particle formation, Atmos. Chem. Phys., 15, 55–78, https://doi.org/10.5194/acp-15-55-2015, 2015.

Sebastian, M., Kanawade, V. P., and Pierce, J. R.: Observation of sub-3nm particles and new particle formation at an urban location in India, Atmos. Environ., 256, 118460, https://doi.org/10.1016/j.atmosenv.2021.118460, 2021.

~~Shang, D., Hu, M., Wang, X., Tang, L., Clusius, P. S., Qiu, Y., Yu, X., Chen, Z., Zhang, Z., Sun, J., Dao, X., Zeng, L., Guo, S., Wu, Z., and Boy, M.: Spatial inhomogeneity of new particle formation in the urban and mountainous atmospheres of the North China Plain during the 2022 Winter Olympics, Atmosphere, 14, 1395, https://doi.org/10.3390/atmos14091395, 2023.~~

Simon, M., Dada, L., Heinritzi, M., Scholz, W., Stolzenburg, D., Fischer, L., Wagner, A. C., Kuerten, A., Rorup, B., He, X.-C., Almeida, J., Baalbaki, R., Baccarini, A., Bauer, P. S., Beck, L., Bergen, A., Bianchi, F., Brakling, S., Brilke, S., Caudillo, L., Chen, D., Chu, B., Dias, A., Draper, D. C., Duplissy, J., El-Haddad, I., Finkenzeller, H., Frege, C., Gonzalez-Carracedo, L., Gordon, H., Granzin, M., Hakala, J., Hofbauer, V., Hoyle, C. R., Kim, C., Kong, W., Lamkaddam, H., Lee, C. P., Lehtipalo, K., Leiminger, M., Mai, H., Manninen, H. E., Marie, G., Marten, R., Mentler, B., Molteni, U., Nichman, L., Nie, W., Ojdanic, A., Onnela, A., Partoll, E., Petaja, T., Pfeifer, J., Philippov, M., Quelever, L. L. J., Ranjithkumar, A., Rissanen, M. P., Schallhart, S., Schobesberger, S., Schuchmann, S., Shen, J., Sipila, M., Steiner, G., Stozhkov, Y., Tauber, C., Tham, Y. J., Tome, A. R., Vazquez-Pufleau, M., Vogel, A. L., Wagner, R., Wang, M., Wang, D. S., Wang, Y., Weber, S. K., Wu, Y., Xiao, M., Yan, C., Ye, P., Ye, Q., Zauner-Wieczorek, M., Zhou, X., Baltensperger, U., Dommen, J., Flagan, R. C., Hansel, A., Kulmala, M., Volkamer, R., Winkler, P. M., Worsnop, D. R., Donahue, N. M., Kirkby, J., and Curtius, J.: Molecular understanding of new-particle formation from α-pinene between -50 and +25°C, Atmos. Chem. Phys., 20, 9183–9207, https://doi.org/10.5194/acp-20-9183-2020, 2020.

Smith, J. N., Barsanti, K. C., Friedli, H. R., Ehn, M., Kulmala, M., Collins, D. R., Scheckman, J. H., Williams, B. J., and McMurry, P. H.: Observations of aminium salts in atmospheric nanoparticles and possible climatic implications, Proc. Natl. Acad. Sci. U. S. A., 107, 6634–6639, https://doi.org/10.1073/pnas.0912127107, 2010.

Stolzenburg, D., Fischer, L., Vogel, A. L., Heinritzi, M., Schervish, M., Simon, M., Wagner, A. C., Dada, L., Ahonen, L. R., Amorim, A., Baccarini, A., Bauer, P. S., Baumgartner, B., Bergen, A., Bianchi, F., Breitenlechner, M., Brilke, S., Mazon, S. B., Chen, D., Dias, A., Draper, D. C., Duplissy, J., El Haddad, I., Finkenzeller, H., Frege, C., Fuchs, C., Garmash, O., Gordon, H., He, X., Helm, J., Hofbauer, V., Hoyle, C. R., Kim, C., Kirkby, J., Kontkanen, J., Kuerten, A., Lampilahti, J., Lawler, M., Lehtipalo, K., Leiminger, M., Mai, H., Mathot, S., Mentler, B., Molteni, U., Nie, W., Nieminen, T., Nowak, J. B., Ojdanic, A., Onnela, A., Passananti, M., Petaja, T., Quelever, L. L. J., Rissanen, M. P., Sarnela, N., Schallhart, S., Tauber, C., Tome, A., Wagner, R., Wang, M., Weitz, L., Wimmer, D., Xiao, M., Yan, C., Ye, P., Zha, Q., Baltensperger, U., Curtius, J., Dommen, J., Flagan, R. C., Kulmala, M., Smith, J. N., Worsnop, D. R., Hansel, A., Donahue, N. M., and Winkler, P. M.: Rapid growth of organic aerosol nanoparticles over a wide tropospheric temperature range, Proc. Natl. Acad. Sci. U. S. A., 115, 9122–9127, https://doi.org/10.1073/pnas.1807604115, 2018.

Tröstl, J., Chuang, W. K., Gordon, H., Heinritzi, M., Yan, C., Molteni, U., Ahlm, L., Frege, C., Bianchi, F., Wagner, R., Simon, M., Lehtipalo, K., Williamson, C., Craven, J. S., Duplissy, J., Adamov, A., Almeida, J., Bernhammer, A.-K., Breitenlechner, M., Brilke, S., Dias, A., Ehrhart, S., Flagan, R. C., Franchin, A., Fuchs, C., Guida, R., Gysel, M., Hansel, A., Hoyle, C. R., Jokinen, T., Junninen, H., Kangasluoma, J., Keskinen, H., Kim, J., Krapf, M., Kuerten, A., Laaksonen, A., Lawler, M., Leiminger, M., Mathot, S., Moehler, O., Nieminen, T., Onnela, A., Petaejae, T., Piel, F. M., Miettinen, P., Rissanen, M. P.,

Rondo, L., Sarnela, N., Schobesberger, S., Sengupta, K., Sipila, M., Smith, J. N., Steiner, G., Tome, A., Virtanen, A., Wagner, A. C., Weingartner, E., Wimmer, D., Winkler, P. M., Ye, P., Carslaw, K. S., Curtius, J., Dommen, J., Kirkby, J., Kulmala, M., Riipinen, I., Worsnop, D. R., Donahue, N. M., and Baltensperger, U.: The role of low-volatility organic compounds in initial particle growth in the atmosphere, Nature, 533, 527–531, https://doi.org/10.1038/nature18271, 2016.

Victor, J. N., Buchunde, P., Sebastian, M., Kanawade, V. P., Siingh, D., Mukherjee, S., Potdar, S. S., Dharmaraj, T., and Pandithurai, G.: Characteristics of new particle formation events in a mountain semi-rural location in India, Atmos. Environ., 324, 120414, https://doi.org/10.1016/j.atmosenv.2024.120414, 2024.

Wang, Y., Yang, G., Lu, Y., Liu, Y., Chen, J., and Wang, L.: Detection of gaseous dimethylamine using vocus proton-transfer-reaction time-of-flight mass spectrometry, Atmos. Environ., 243, 117875, https://doi.org/10.1016/j.atmosenv.2020.117875, 2020.

~~Wu, Y., Huo, J., Yang, G., Wang, Y., Wang, L., Wu, S., Yao, L., Fu, Q., and Wang, L.: Measurement report: Production and loss of atmospheric formaldehyde at a suburban site of Shanghai in summertime, Atmos. Chem. Phys., 23, 2997–3014, https://doi.org/10.5194/acp-23-2997-2023, 2023.~~

Xiao, M., Hoyle, C. R., Dada, L., Stolzenburg, D., Kuerten, A., Wang, M., Lamkaddam, H., Garmash, O., Mentler, B., Molteni, U., Baccarini, A., Simon, M., He, X.-C., Lehtipalo, K., Ahonen, L. R., Baalbaki, R., Bauer, P. S., Beck, L., Bell, D., Bianchi, F., Brilke, S., Chen, D., Chiu, R., Dias, A., Duplissy, J., Finkenzeller, H., Gordon, H., Hofbauer, V., Kim, C., Koenig, T. K., Lampilahti, J., Lee, C. P., Li, Z., Mai, H., Makhmutov, V., Manninen, H. E., Marten, R., Mathot, S., Mauldin, R. L., Nie, W., Onnela, A., Partoll, E., Petaja, T., Pfeifer, J., Pospisilova, V., Quelever, L. L. J., Rissanen, M., Schobesberger, S., Schuchmann, S., Stozhkov, Y., Tauber, C., Tham, Y. J., Tome, A., Vazquez-Pufleau, M., Wagner, A. C., Wagner, R., Wang, Y., Weitz, L., Wimmer, D., Wu, Y., Yan, C., Ye, P., Ye, Q., Zha, Q., Zhou, X., Amorim, A., Carslaw, K., Curtius, J., Hansel, A., Volkamer, R., Winkler, P. M., Flagan, R. C., Kulmala, M., Worsnop, D. R., Kirkby, J., Donahue, N. M., Baltensperger, U., El Haddad, I., and Dommen, J.: The driving factors of new particle formation and growth in the polluted boundary layer, Atmos. Chem. Phys., 21, 14275–14291, https://doi.org/10.5194/acp-21-14275-2021, 2021.

Xiao, S., Wang, M. Y., Yao, L., Kulmala, M., Zhou, B., Yang, X., Chen, J. M., Wang, D. F., Fu, Q. Y., Worsnop, D. R., and Wang, L.: Strong atmospheric new particle formation in winter in urban Shanghai, China, Atmos. Chem. Phys., 15, 1769–1781, https://doi.org/10.5194/acp-15-1769-2015, 2015.

Yan, C., Yin, R., Lu, Y., Dada, L., Yang, D., Fu, Y., Kontkanen, J., Deng, C., Garmash, O., Ruan, J., Baalbaki, R., Schervish, M., Cai, R., Bloss, M., Chan, T., Chen, T., Chen, Q., Chen, X., Chen, Y., Chu, B., Dällenbach, K., Foreback, B., He, X., Heikkinen, L., Jokinen, T., Junninen, H., Kangasluoma, J., Kokkonen, T., Kurppa, M., Lehtipalo, K., Li, H., Li, H., Li, X., Liu, Y., Ma, Q., Paasonen, P., Rantala, P., Pileci, R. E., Rusanen, A., Sarnela, N., Simonen, P., Wang, S., Wang, W., Wang, Y., Xue, M., Yang, G., Yao, L., Zhou, Y., Kujansuu, J., Petäjä, T., Nie, W., Ma, Y., Ge, M., He, H., Donahue, N. M., Worsnop, D. R., Kerminen, V.-M., Wang, L., Liu, Y., Zheng, J., Kulmala, M., Jiang, J., and Bianchi, F.: The synergistic role of sulfuric acid, bases, and oxidized organics governing new-particle formation in Beijing, Geophys. Res. Lett., 48, e2020GL091944, https://doi.org/10.1029/2020GL091944, 2021.

Yao, L., Wang, M.-Y., Wang, X.-K., Liu, Y.-J., Chen, H.-F., Zheng, J., Nie, W., Ding, A.-J., Geng, F.-H., Wang, D.-F., Chen, J.-M., Worsnop, D. R., and Wang, L.: Detection of atmospheric gaseous amines and amides by a high-resolution time-of-flight chemical ionization mass spectrometer with protonated ethanol reagent ions, Atmos. Chem. Phys., 16, 14527–14543, https://doi.org/10.5194/acp-16-14527-2016, 2016.

Yao, L., Garmash, O., Bianchi, F., Zheng, J., Yan, C., Kontkanen, J., Junninen, H., Mazon, S. B., Ehn, M., Paasonen, P., Sipila, M., Wang, M., Wang, X., Xiao, S., Chen, H., Lu, Y., Zhang, B., Wang, D., Fu, Q., Geng, F., Li, L., Wang, H., Qiao, L., Yang, X., Chen, J., Kerminen, V.-M., Petaja, T., Worsnop, D. R., Kulmala, M., and Wang, L.: Atmospheric new particle formation from sulfuric acid and amines in a Chinese megacity, Science, 361, 278–281, https://doi.org/10.1126/science.aao4839, 2018.

Yin, R., Yan, C., Cai, R., Li, X., Shen, J., Lu, Y., Schobesberger, S., Fu, Y., Deng, C., Wang, L., Liu, Y., Zheng, J., Xie, H., Bianchi, F., Worsnop, D. R., Kulmala, M., and Jiang, J.: Acid-base clusters during atmospheric new particle formation in urban Beijing, Environ. Sci. Technol., 55, 10994–11005, https://doi.org/10.1021/acs.est.1c02701, 2021.

Yu, H., Zhou, L., Dai, L., Shen, W., Dai, W., Zheng, J., Ma, Y., and Chen, M.: Nucleation and growth of sub-3 nm particles in the polluted urban atmosphere of a megacity in China, Atmos. Chem. Phys., 16, 2641–2657, https://doi.org/10.5194/acp-16-

2641-2016, 2016.

~~Zapadinsky, E., Passananti, M., Myllys, N., Kurtén, T., and Vehkamäki, H.: Modeling on fragmentation of clusters inside a mass spectrometer, J. Phys. Chem. A, 123, 611–624, https://doi.org/10.1021/acs.jpca.8b10744, 2019.~~

Zhao, B., Donahue, N. M., Zhang, K., Mao, L., Shrivastava, M., Ma, P.-L., Shen, J., Wang, S., Sun, J., Gordon, H., Tang, S., Fast, J., Wang, M., Gao, Y., Yan, C., Singh, B., Li, Z., Huang, L., Lou, S., Lin, G., Wang, H., Jiang, J., Ding, A., Nie, W., Qi, X., Chi, X., and Wang, L.: Global variability in atmospheric new particle formation mechanisms, Nature, 631, 98–105, https://doi.org/10.1038/s41586-024-07547-1, 2024.

Zhou, Y., Hakala, S., Yan, C., Gao, Y., Yao, X., Chu, B., Chan, T., Kangasluoma, J., Gani, S., Kontkanen, J., Paasonen, P., Liu, Y., Petaja, T., Kulmala, M., and Dada, L.: Measurement report: New particle formation characteristics at an urban and a mountain station in northern China, Atmos. Chem. Phys., 21, 17885–17906, https://doi.org/10.5194/acp-21-17885-2021, 2021.